

22. SITE 946¹

Shipboard Scientific Party²

HOLE 946A

Date occupied: 18 May 1994
Date departed: 18 May 1994
Time on hole: 2 days, 16 hr, 15 min
Position: 6°56.977'N, 47°55.161'W
Bottom felt (drill pipe measurement from rig floor, m): 4111.5
Distance between rig floor and sea level (m): 11.40
Water depth (drill pipe measurement from sea level, m): 4100.1
Penetration (m): 275.00
Number of cores (including cores having no recovery): 29
Total length of cored section (m): 275.00
Total core recovered (m): 172.18
Core recovery (%): 62
Oldest sediment cored:
Depth (mbsf): 275.00
Nature: Silty clay
Earliest age: Pleistocene

Principal results: Site 946 (proposed Site AF-24) is located near the transition from the middle to the lower Amazon Fan. It is one of a series of sites designed to characterize the development of the most recently active channel of the Amazon Fan (the Amazon Channel). The hole penetrated the Amazon levee and the underlying highly reflective seismic units characteristic of the lower fan. Site 945 was located 1.2 km to the west on the adjacent channel floor.

The site was selected from a *Conrad* seismic-reflection profile (C2514; 0210UTC on 18 Dec. 1984). The precise position was confirmed by a pre-site survey from *JOIDES Resolution*.

Hole 946A was cored by APC to 140.0 mbsf, then by XCB to 275.0 mbsf. APC recovery was 127.91 m (91.4%), and XCB recovery was 44.3 m (32.8%). Temperature measurements made at the mud line and at 64 mbsf (ADARA) show a mean geothermal gradient of 43°C/km. There was gas expansion in many cores. Methane was found throughout the hole, but higher hydrocarbons were not detected. The site was logged with the Quad-combination and FMS tool strings from 78 to 274 mbsf.

Seven lithologic units are recognized:

Unit I (0–0.45 mbsf) is a Holocene bioturbated, foraminifer-nannofossil clay, similar to Unit I at other Leg 155 sites.

Unit II (0.45–1.18 mbsf) consists of clay with burrow mottles and faint color banding.

Unit III (1.18–128.72 mbsf) consists of mud, silt, and sand beds, with a general trend to thicker sand beds and sand beds with abundant mud clasts downhole. The thickness of some sand beds may have been inflated by sand flow during coring. The unit is subdivided based on the relative abundance of sand beds. Subunit IIIA (1.18–4.42 mbsf) comprises mud

with numerous graded beds of fine sand to silt, on average 6 cm thick, making up 30% of the subunit. Subunit IIIB (4.42–24.72 mbsf) contains bioturbated mud with numerous laminae and thin beds of silt. Subunit IIIC (24.72–128.72 mbsf) consists of mud with numerous laminae and beds of silt and sand. Silt beds are as thick as 75 cm and are graded. Sand beds have abundant 1- to 10-cm mud clasts and generally grade upward from poorly sorted fine sand to silt, although rare medium sand is present. Some of the sand beds appear to be more than 1 m thick. The alternation of sandier and siltier intervals below 67 mbsf can be correlated with similar alternations below 12 mbsf at Site 945. The upper part of Unit III (to 24 mbsf) is correlated seismically with the Amazon Channel levee, and the middle part (to 45 mbsf) with an underlying levee. The lower part of the unit corresponds to lower fan sand over which the levees have prograded. When deposited, these sand beds were located beyond the contemporary channel termination.

Unit IV (128.72–155.82 mbsf) consists of a series of intervals of mud with silt laminae and minor beds of silt interspersed with beds of calcareous clay that have carbonate contents of 7%–36%. The content of organic carbon (0.4%) and nitrogen (0.1%) is low in the calcareous intervals. Burrow mottles are common to abundant throughout this unit. The top of the unit is an erosional boundary overlain by a 50-cm-thick graded bed of medium to fine sand. A thin calcareous clay occurs at 133.25–133.75 mbsf. From 140 to 149 mbsf, several 20- to 30-cm-thick intervals of greenish gray nannofossil-foraminifer-rich clay alternate with dark gray foraminifer-bearing clay.

Unit V (155.82–211.37 mbsf) had only 21% recovery and most of its sand was highly disturbed by coring. The upper 5 m of the unit comprises mud with thin to thick silt beds. Below this, recovery was sparse and consists of two cores of abundant mud clasts in a poorly sorted matrix of fine to medium sand. Wireline log data suggest that much of this unit consists of “clean” sand, which below 180 mbsf forms three coarsening-upward sequences. FMS images show packets of 0.5- to 1-m-thick sand beds. The data suggest that individual sand packets are thicker than in the lower part of Unit III, which was also logged, but muddy intervals are thicker and less silty in Unit V. Seismically, this unit and the overlying Unit IV are correlated with the feather edge of either the Middle or the Lower Levee Complex.

Unit VI (211.37–220.0 mbsf) consists of greenish gray calcareous clay interbedded with dark gray mud with laminae and thin beds of silt. Burrow mottling is common. The top of the unit is an irregular erosional surface, and the overlying sand contains rip-up clasts from this unit.

Unit VII (220.0–273.67 mbsf) had less than 19% recovery, almost all of which was in two cores from the top and base of the unit that consist of mud with silt laminae, similar to levee sequences recovered elsewhere during Leg 155. Wireline logs, however, show that from 218 to 250 mbsf, the unit consists predominantly of sand. From 250 to 262 mbsf, log response suggests alternating sand and mud in a thinning-upward sequence, which is underlain by a predominantly muddy sequence below 262 mbsf, corresponding to the mud with silt laminae recovered in Core 29X. FMS images suggest sand-bed thicknesses of 3–5 m at the top of the unit, decreasing downhole.

Foraminifers and nannofossils are well preserved and abundant in the calcareous clays of Units I, IV, and VI. Otherwise, microfossils are sparse, and nannofossils are commonly etched. Our preliminary shipboard study suggests that Unit IV nannofossil assemblages are of Zone CN15a and are

¹Flood, R.D., Piper, D.J.W., Klaus, A., et al., 1995. *Proc. ODP, Init. Repts.*, 155: College Station, TX (Ocean Drilling Program).

²Shipboard Scientific Party is as given in the list of participants in the contents.

thus similar to those in Units III, IV, and V at Site 942. Unit VI nannofossil assemblages are dominated by *Gephyrocapsa* and are referred to Zone CN14b. *P. obliquiloculata* is found in a sandy interval at 53.5 mbsf in Unit III and is probably reworked. Units IV and VI contain interglacial foraminifers including *G. menardii*, *G. tumida*, and *G. tumida flexuosa*. *G. hexagonus* is present in Unit IV.

Two anomalous intervals of remanence direction and intensity, interpreted as geomagnetic excursions, occur at 101.5 mbsf and 133.5 mbsf, the latter in an interval of calcareous clay. On the basis of the pattern of their remanence behavior, these are interpreted as the Lake Mungo (30 ka) Excursion and the Blake (105 ka) Event. Oscillations in paleomagnetic declination and inclination, interpreted as secular variation, are best developed from 10 to 13 mbsf, with a wavelength of 0.25 m.

Individual sand beds and packets of mud with silt beds can be tentatively correlated between Site 945 and the upper 110 m of Site 946, using continuity of seismic reflections as a guide. The depth below seafloor of any particular feature is about 55 m greater at Site 946. This lateral continuity of sandy units implies that these sediment beds were deposited on the lower fan beyond the limit of strongly channelized flow.

This site was a fitting end to a highly successful leg. It is the only site wherein two major units were recovered that contained interglacial calcareous clay beds, with a thick sandy interval (Unit V) between them. The presence of the Blake Event and the tentative biostratigraphic correlation with Site 942 allow us to correlate Unit IV of Site 946 with the interglacial of isotopic Stage 5. Units IV and VI have different nannofossil and foraminifer assemblages and are separated by a thick sand unit. Unit VI therefore appears to date from an earlier interglacial and may correlate biostratigraphically with the interglacial sediment beds near the base of Sites 931 and 933. The excellent recovery to 160 mbsf and the remarkably good correlation between sands in Sites 945 and 946 provide unparalleled sedimentological detail of the sandy depositional lobe beyond the termination of the fan channel.

SETTING AND OBJECTIVES

Introduction

Site 946 (proposed Site AF-24) is located near the transition from the middle to lower fan at 4100 m. It is one of a series of sites designed to characterize the development of the most recently active channel of the Amazon Fan (the Amazon Channel). The hole penetrated the Amazon levee and the underlying highly reflective seismic units interpreted as lower-fan deposits. The nearby channel was sampled at Site 945.

Setting

Site 946 is located on the eastern (right) levee of the Amazon Channel, about 1 km from the channel axis (see Fig. 1 of "Site 945" chapter, this volume). Seismic records suggest that the fan in this area is built of interfingering seismic units. The thicker, more reflective units appear to correlate with the high-amplitude reflection packets (HARPs) identified up-fan. The thinner, less reflective units appear to be levee deposits and disappear down-fan, resulting in a lower fan dominated by the more reflective units (Flood et al., 1991). The base of the modern channel levee can be identified on the 3.5-kHz profile (see Fig. 3 of "Site 945" chapter, this volume). The channel geometry and near-surface sedimentation patterns in this area have been determined on the basis of multibeam bathymetric and piston core data (Flood et al., 1991; Pirmez, 1994). Site 946 is where the most recently active segment of the Amazon Channel branched off from an earlier leveed channel that continues to the west.

The site was selected from a *Conrad* seismic profile (C2514; 0210UTC on 18 Dec. 1984). We located Site 946 at a similar position on our *JOIDES Resolution* profile (1859UTC on 17 May 1994; Fig. 2 of "Site 945" chapter, this volume).

Site 946 samples sequences similar to those recovered at Site 944, although the relative proportions of different units have changed in

this site at the middle/lower fan transition. The Amazon Channel levee, at this point, is much thinner (30 ms). The levee record at this site needs to be compared with the records from Sites 939, 940, 935, 936, and 944 to characterize the growth of these most recent levees. The underlying HARP unit is a 170-ms-thick reflective sequence that can be correlated to Sites 945, 944, 936, and 935. The Unit R Debris Flow, which underlies the HARP unit up-fan, cannot be correlated seismically with this site. Instead, a less reflective interval 60 ms thick that appears to correspond to the Middle Levee Complex and/or the Upper Levee Complex at up-fan sites underlies the HARP layer here. A second high-reflectivity unit, which may represent a deeper HARP unit associated with the Lower Levee Complex, underlies the less reflective interval. The less reflective seismic interval pinches out down-fan, and the stacked high-reflectivity units appear to form the lower fan in this area.

Objectives

The principal objectives at Site 946 were to:

1. Sample the Amazon levee deposits to characterize turbidity current dynamics and to compare the sediment record here with that of other near-channel sites at several depths along the 700-km-long Amazon Channel, and with the adjacent site in the channel (Site 945).
2. Sample the multiple HARPs that underlie the channel for comparison with up-fan units.
3. Characterize the downslope evolution of Unit R Debris Flow by sampling the stratigraphically equivalent unit at this site. A sedimentary record of Unit R was anticipated even though it is not seismically identified here.
4. Sample the relatively thin, less reflective interval that correlates with the Lower Levee Complex to verify the correlation and to compare the deep and surficial levees.
5. Sample the underlying HARP units for comparison to the near-surface HARPs.

The logging objectives at Site 946 were to characterize the upper and lower HARP units, the intervening less reflective unit, and the possible debris-flow equivalent by their log response, and to establish thicknesses and patterns of sand beds that may be poorly recovered by coring.

OPERATIONS

Transit: Site 945 to Site 946 (AF-24)

The ~1.0-nmi transit from Site 945 to Site 946 was made in dynamic positioning mode and took about 1.1 hr. At 1034 hr 18 May, we deployed a beacon at 6°56.978'N, 47°55.156'W. The precise position was selected from a seismic-reflection survey conducted prior to Site 945.

Hole 946A

We positioned the bit at 4107.0 mbrf and attempted to spud Hole 946A. It appeared that about 4 m of sediment had fallen out of the liner. We repositioned the bit at 4109.0 mbrf and spudded Hole 946A at 1300 hr 18 May. Core 1H recovered 7.05 m, and the mud line was defined to be at 4111.5 mbrf. The distance from sea level to rig floor, which depends on the ship's draft, was 11.35 m for Hole 946A. Cores 1H through 15H were taken from 4111.5 to 4251.5 mbrf (0–140.0 mbsf) and recovered 127.51 m (91.1%; Table 1). Three core liners failed, including an imploded bottom, a split bottom, and a burst top. Cores 3H through 15H were oriented using the Tensor tool. ADARA heat-flow measurements were taken during Cores 5H (bad data) and 7H. Core 7H misfired when the shear pins failed to shear with 3000 psi. The formation was predominantly loose sand. Parts of Cores 2H,

Table 1. Site 946 coring summary.

Core	Date (1994)	Time (UTC)	Depth (mbsf)	Length cored (m)	Length recovered (m)	Recovery (%)
155-946A-						
1H	May 18	1720	0.0–7.0	7.0	7.05	101.0
2H	May 18	1810	7.0–16.5	9.5	9.50	100.0
3H	May 18	1905	16.5–26.0	9.5	9.80	103.0
4H	May 18	2005	26.0–35.5	9.5	9.86	104.0
5H	May 18	2120	35.5–45.0	9.5	9.87	104.0
6H	May 18	2210	45.0–54.5	9.5	8.60	90.5
7H	May 19	0020	54.5–64.0	9.5	9.60	101.0
8H	May 19	0115	64.0–73.5	9.5	10.01	105.3
9H	May 19	0215	73.5–83.0	9.5	9.33	98.2
10H	May 19	0310	83.0–92.5	9.5	2.65	27.9
11H	May 19	0425	92.5–102.0	9.5	9.76	103.0
12H	May 19	0535	102.0–111.5	9.5	8.06	84.8
13H	May 19	0640	111.5–121.0	9.5	5.95	62.6
14H	May 19	0745	121.0–130.5	9.5	10.85	114.2
15H	May 19	0845	130.5–140.0	9.5	7.02	73.9
16X	May 19	1015	140.0–149.6	9.6	9.36	97.5
17X	May 19	1120	149.6–159.2	9.6	9.76	101.0
18X	May 19	1225	159.2–168.8	9.6	1.71	17.8
19X	May 19	1330	168.8–178.5	9.7	0.11	1.1
20X	May 19	1430	178.5–188.2	9.7	0.00	0.0
21X	May 19	1545	188.2–197.8	9.6	5.10	53.1
22X	May 19	1655	197.8–207.5	9.7	0.03	0.3
23X	May 19	1815	207.5–217.1	9.6	4.86	50.6
24X	May 19	1920	217.1–226.7	9.6	4.63	48.2
25X	May 19	2025	226.7–236.4	9.7	0.00	0.0
26X	May 19	2125	236.4–246.1	9.7	0.00	0.0
27X	May 19	2240	246.1–255.7	9.6	0.00	0.0
28X	May 19	2355	255.7–265.4	9.7	0.44	4.5
29X	May 20	0215	265.4–275.0	9.6	8.27	86.1
Coring totals				275.0	172.2	62.6

Note: An expanded version of this coring summary table that includes lengths and depths of sections, location of whole-round samples, and comments on sampling disturbance is included on the CD-ROM in the back pocket of this volume.

14H, and 15H were disturbed as a result of either gas-induced extrusion of core from the liner onto the rig floor or collapsed core liners.

XCB Cores 16X through 29X were taken from 4251.5 to 4386.5 mbrf (140.0–275.0 mbsf), coring 135.0 m and recovering 44.11 m (32.7%). The overall APC/XCB recovery was 62.4%. Recovery was poor in what we infer to be loose sand.

In preparation for logging, we circulated a 20-barrel and then a 30-barrel sepiolite/seawater mud sweep, and the pipe was pulled up to 79.0 mbsf with negligible overpull. When running the pipe back to the bottom of the hole, we encountered 7 m of soft fill on the bottom. We dropped the go-devil to open the LFV and filled the hole with 8.8 ppg sepiolite mud. The pipe was pulled back up to 97.0 mbsf for logging. The bit was pulled up to 78 mbsf to log the upper hole at the end of each logging run. Logs were run as follows:

The Quad combo was run in to 4385.0 mbrf (273.5 mbsf; there was 1.5 m of fill) in 5.5 hr. Initially, the FMS string would not pass through the bit, and the drill string was stuck. The drill string was freed with 100,000-lb overpull by pumping 150 gpm at 3000 psi. Then, the drill string was pulled up to 79 mbsf, and the FMS tool passed through the bit into the hole. The FMS log was run in to 4385.0 mbrf (273.5 mbsf; there was 1.5 m of fill) in 5.2 hr.

The bit cleared the seafloor at 1820 hr 20 May. The beacon was retrieved at 1952 hr 20 May. The bit cleared the rotary table at 0242 hr 21 May; the drill floor, thrusters, and hydrophones were secured at 0352 hr. The BHA was laid down so Leg 156 could start with a new BHA for a "Measurement-While-Drilling" (MWD) experiment. The sea voyage began at 0400 hr 21 May.

Sea Voyage from Site 946 to Barbados

The sea voyage from Site 946 to Barbados covered 788 nmi in about 74 hr. Leg 155 ended with the first line ashore in Barbados at 0615 hr 24 May.

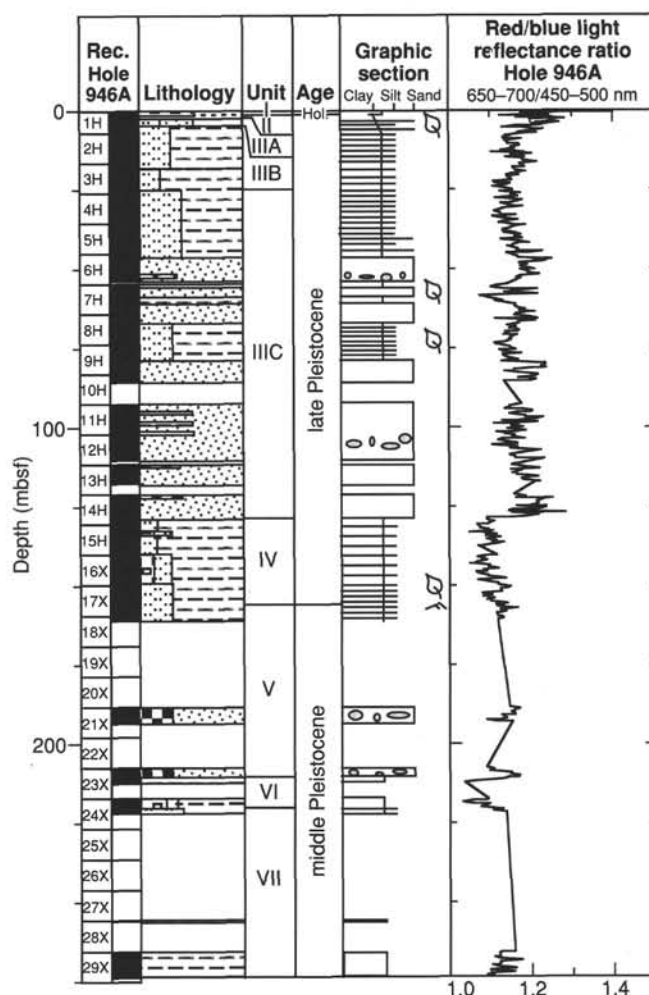


Figure 1. Composite stratigraphic section for Site 946 showing core recovery, a simplified summary of lithology, depths of unit boundaries, age, a graphic section with generalized grain-size and bedding characteristics (simplified from Fig. 2), and downhole variations in light-reflectance values. The lithologic symbols are explained in Figure 1 of the "Explanatory Notes" chapter, this volume.

LITHOSTRATIGRAPHY

Introduction

Hole 946A, which is near the down-fan termination of the eastern levee of the main Amazon Channel, recovered sediment from a maximum depth of 273.67 mbsf. Recovery was variable downhole, ranging from 0% to over 100% with an average of 62.6% (Figs. 1 and 2). Expansion of methane gas during core recovery commonly affected the sediment by disrupting the primary sedimentary structures in many silt and sand beds, and by producing void spaces within some of the core sections (see "Lithostratigraphy" section in the "Explanatory Notes" chapter, this volume). Some sediment intervals possess a honeycomb or "mousse" texture (e.g., Fig. 16 of "Site 945" chapter, this volume), which might indicate that they contained gas hydrates in the subsurface. In addition, some of the recovered sand was soupy and therefore structureless, probably as a result of "flow-in" induced by hydraulic piston coring. Intervals that might have been thickened by "flow-in" are primarily the thick sand that forms the lower parts of some cores (Fig. 2).

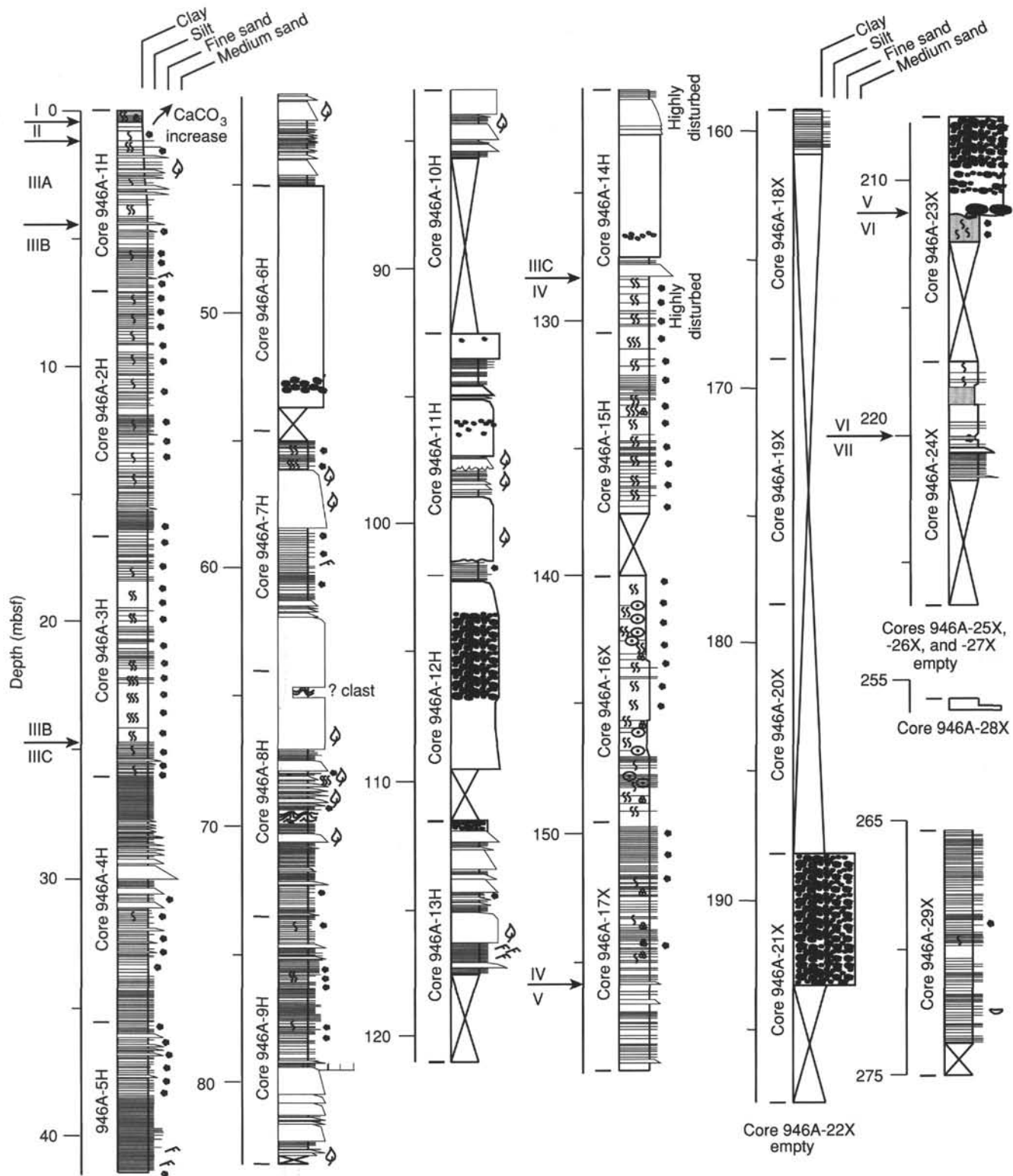


Figure 2. Graphic sedimentological columns for Site 946 showing grain-size variation (width of columns), bed thickness, and sedimentary structures; symbols and preparation of these columns are explained in the "Lithostratigraphy" section of the "Explanatory Notes" chapter, this volume. Arrows indicate the positions of unit and subunit boundaries. The upper part of the column is shown in the longitudinal profile of the foldout (back pocket, this volume) to show the down-fan changes in levee deposits.

Description of Lithostratigraphic Units

Unit I

Interval: 155-946A-1H-1, 0–45 cm
Age: Holocene
Depth: 0.00–0.45 mbsf

Unit I consists of 0.45 m of calcareous clay similar to that observed at most other sites on the surface of the Amazon Fan. A 34-cm-thick, pale brown (10YR 6/3) foraminifer-nannofossil clay overlies a grayish brown (10YR 5/2) calcareous clay, with faint color banding. The base of Unit I is a 1-cm-thick dark brown (7.5YR 3/2) diagenetic, iron-rich crust. Similar diagenetic, iron-rich layers or crusts were analyzed previously and correlated throughout the Amazon Fan and adjacent Guiana Basin (e.g., Damuth, 1977; see "Introduction" chapter, this volume).

Unit II

Interval: 155-946A-1H-1, 45–118 cm
Age: Holocene to ?late Pleistocene
Depth: 0.45 to 1.18 mbsf

Unit II consists predominantly of a light olive brown (2.5Y 5/2) clay that grades downhole to a dark grayish brown (2.5Y 4/2) clay with burrow mottles and faint color banding (Figs. 1 and 2). The carbonate content near the color change in this unit is 0.5%.

Unit III

Interval: 155-946A-1H-1, 118 cm, through -14H-6, 69 cm
Age: late Pleistocene
Depth: 1.18 to 128.72 mbsf

The top of Unit III corresponds to the upper limit of silt and sand beds at this site. The very dark grayish brown (2.5Y 3/2) silt and sand beds are interbedded with very dark gray (5Y 4/1) clay and dark olive gray (5Y 3/1) silty clay. There is a general trend to thicker sand beds and sand beds with abundant clay and silty clay clasts downhole (Fig. 5 of "Site 943" chapter, this volume). Shipboard determinations of the carbonate content of Unit III averaged 2.3%, except for one measurement of 12.8% in a 2-cm-thick carbonate-rich layer at 55.40 mbsf (Sample 946A-7H-1, 90 cm), probably siderite. Unit III is divided into subunits based on the relative abundance of sand beds that form coarse-grained intervals as much as 8 m thick, although the in-place thickness of many sand beds likely has been inflated by "flow-in" during APC coring.

Subunit IIIA

Subunit IIIA extends from 1.18 to 4.42 mbsf (interval 946A-1H-1, 118 cm, through -1H-3, 142 cm). This thin subunit consists of dark gray (5Y 4/1) clay with numerous graded beds of very dark grayish-brown (2.5Y 3/2) fine sand to silt (Fig. 3). About 30% of the subunit is composed of sand and silt layers. Bed thickness ranges from 2 to 14 cm with an average of 6 cm, which distinguishes this subunit from the underlying one where the beds are no coarser than silt and rarely thicker than 6 cm. The clay interbeds in subunit IIIA are color banded and show a moderate density of burrow mottles.

Subunit IIIB

Subunit IIIB extends from 4.42 to 24.72 mbsf (interval 946A-1H-3, 142 cm, through -3H-6, 72 cm) and is characterized by dark gray (5Y 4/1) to very dark gray (5Y 3/1) silty clay with numerous silt laminae and thin beds of silt. Black burrow mottles and color banding are present throughout the subunit, but the mottling is more extensive downhole where the abundance of silt beds decreases (Fig. 2). Mud turbidites, 2 to 5 cm thick, are common in this subunit (Fig. 4).

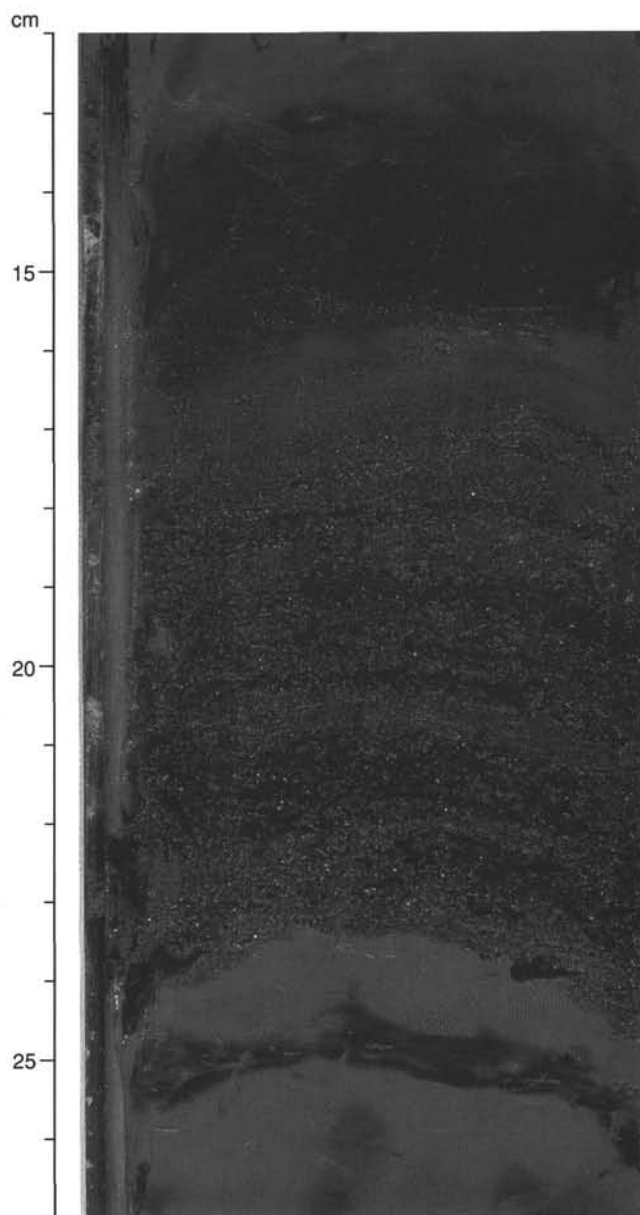


Figure 3. Normally graded fine sand to silt turbidite of Subunit IIIA with leaf fragments along the base of the bed and dark bands rich in organic detritus at several levels (155-946A-1H-3, 12–27 cm).

Subunit IIIC

Subunit IIIC extends from 24.72 to 128.72 mbsf (interval 946A-3H-6, 72 cm, through -14H-6, 69 cm). This subunit consists of dark to very dark gray (5Y 4/1 to 5Y 3/1) silty clay with numerous laminae and beds of silt and thick sand; many of the beds have abundant mud clasts with diameters of 1–10 cm. Plant debris is common in most of the silt and sand beds, occurring both as fragments ranging from a few millimeters to a centimeter in size (Fig. 5) and as fibers forming a significant portion of muddy silt beds that are several centimeters thick.

The average number of laminae and beds of silt per meter exceeds 20 in some intervals. Color banding and burrow mottles extend throughout the subunit and are most noticeable in those intervals with fewer silt layers (Fig. 2). Silt beds are as thick as 75 cm and common-

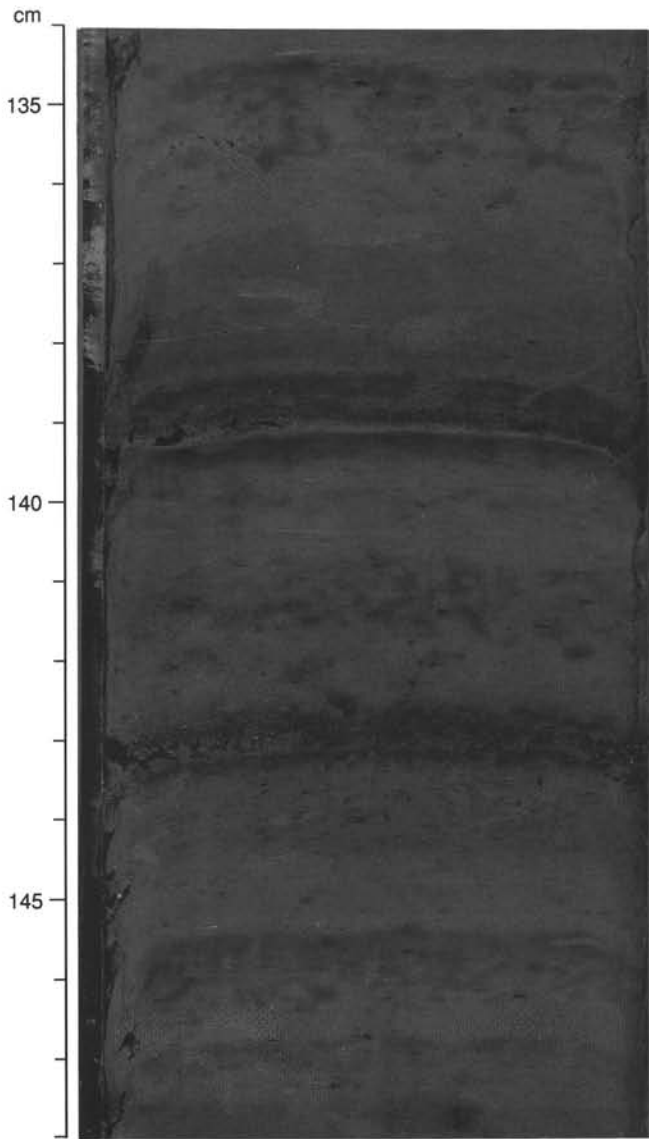


Figure 4. Mud turbidites of Subunit IIIB, each with a lighter colored basal part and a burrowed upper part characterized by dark mottles (e.g., 145.5 to 147 cm). The turbidites from 134.5 to 139 cm and 141 to 143 cm graded into basal silt laminae 2- to 3-mm thick (155-946A-2H-1, 134-148 cm).

ly are graded. Sand beds generally grade from poorly sorted fine sand to silt. The thickness of some structureless sand beds is difficult to determine because they may have been thickened by "flow-in" during coring. Alternatively, the lack of structure in some of these beds may be entirely the result of (1) rapid deposition from high-concentration sediment gravity flows, and/or (2) gas expansion during core retrieval. Below about 85 mbsf, most thick sand beds have abundant mud clasts (Fig. 6).

Several sand turbidites in Subunit IIIC directly overlie a clayey silt layer, the latter typically several centimeters thick (Figs. 5 and 7). Both the sand and clayey silt layers have sharp bases. These paired sand and clayey silt layers may be genetically related, and similar bed couplets occur at Site 945 (see Fig. 15A [64.5 to 66.5 cm] and Fig. 15B [40.5 to 42.0 cm] of "Site 945" chapter, this volume). Wavy beds of cross-laminated silt and sand are also locally common in Subunit IIIC (Fig. 8).

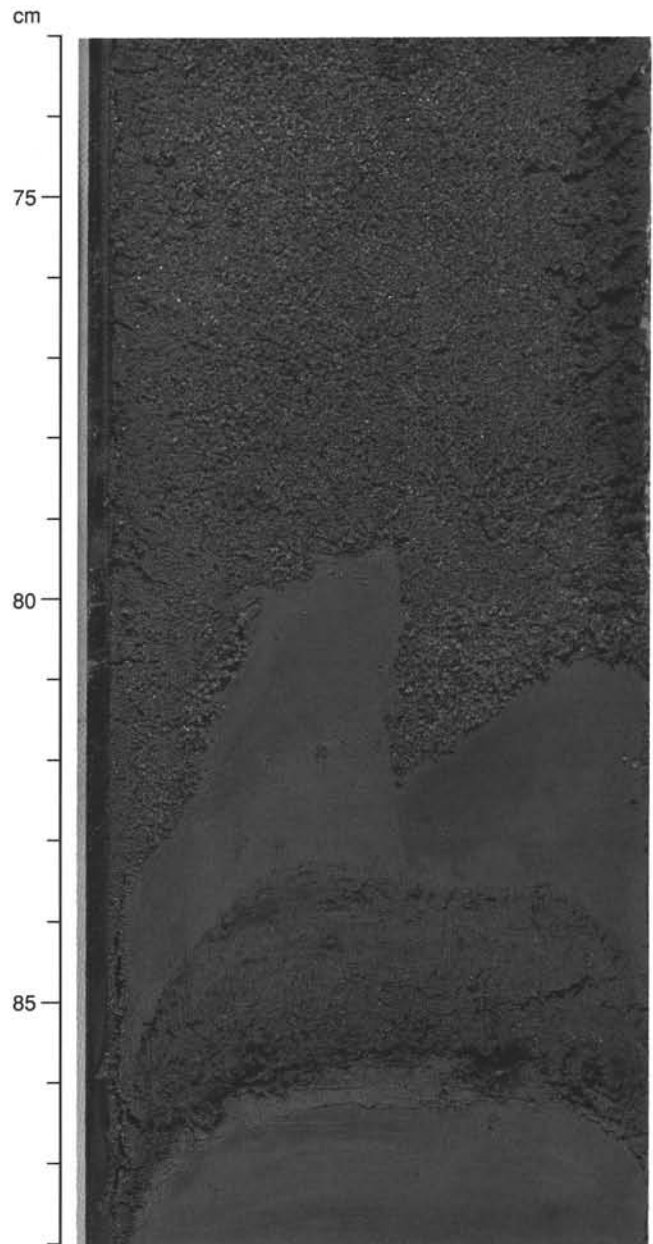


Figure 5. Medium-grained turbidite sand (73 to 82 cm) with basal, irregularly shaped mud clasts (82 to 83.5 cm along core centerline), Subunit IIIC. Underlying the mud clasts is a bed of poorly sorted silt (84 to 86.5 cm) with an organic layer containing leaf fragments 5 mm above its base (155-946A-11H-4, 73-88 cm).

Unit IV

Interval: 155-946A-14H-6, 69 cm, through -17X-5, 22 cm
 Age: late Pleistocene
 Depth: 128.72 to 155.82 mbsf

The top of Unit IV is sharply overlain by a 35-cm-thick sand bed that is normally graded from medium to fine sand. Unit IV consists of a series of intervals of silty clay with silt laminae and minor beds of silt interspersed with intervals of carbonate-rich clay (Fig. 2). Burrow mottles are common to abundant throughout this unit. A black (N2/O) mineral, probably hydrotroilite, is abundant as staining of bur-

row fills, as soft micronodules that are most common within the silty clay intervals, and as prominent bands (Fig. 9); the black staining is ephemeral.

Dark gray to very dark gray (5Y 4/1 to 5Y 3/1) silty clay with silt laminae extends from the top of Unit IV to a 0.50-m-thick foraminifer-rich silty clay between 133.25 and 133.75 mbsf (interval 946A-15X-3, 38–88 cm). Below this interval, very dark gray silty clay with some silt laminae extends downhole to the bottom of Core 946A-15X at 137.52 mbsf. A coring gap of about 1.5 m separates this silty clay from an underlying interval of foraminifer-bearing clay with common burrow mottles and black staining that extends from 140.00 to 148.80 mbsf (interval 946A-16X-1 through -16X-6, 130 cm). This foraminifer-bearing clay includes several 20- to 30-cm-thick intervals of nannofossil-foraminifer clay. The nannofossil-foraminifer clays are light greenish gray to greenish gray (5GY 5/1 to 5GY 4/1), significantly lighter than the dominant silty clay in this unit (Fig. 10). The carbonate content of the silty clays of Unit IV is less below 148.80 mbsf, and the bottom of the unit is placed at the first thick silt bed at 155.82 mbsf (Section 946A-17X-5 at 22 cm). The carbonate content of silty clay intervals in Unit IV averages only 1.7%, but the carbonate-rich intervals contain 6.5% to 35.5% carbonate, with an average of 17.5% for eight samples.

Unit V

Interval: 155-946A-17X-5, 22 cm, through -23X-3, 87 cm
Age: middle Pleistocene
Depth: 155.82 to 211.37 mbsf

Unit V consists of thin to thick silt beds in the upper 5 m and thick intervals of very poorly sorted fine sand, commonly with abundant mud clasts, in the lower part of the unit (Fig. 2). Core recovery in this unit was only 21%, and much of the sand lost its primary sedimentary structure during coring; the in-place bed thicknesses cannot be reliably determined based on the core recovered. Mud clasts in Core 946A-21X are grain supported in a matrix of poorly sorted medium sand. Clasts include carbonate-rich clays and silty clays with color banding and silt laminae (Fig. 11). In interval 946A-23X-1, 0 cm, through -23X-3, 87 cm, the abundant mud clasts are supported by a matrix of poorly sorted, fine to medium sand. The carbonate content of the upper part of Unit V is 3.6% based on one sample.

Unit VI

Interval: 155-946A-23X-3, 87 cm, through -24X-2, 140 cm
Age: middle Pleistocene
Depth: 211.37 to 220.00 mbsf

The top of Unit VI is an irregular erosional surface; the sediment gravity flow that deposited the basal sand layer of Unit V apparently ripped up several clasts from the top of Unit VI. Unit VI is dominantly greenish gray and dark greenish gray (5GY 5/1 and 5GY 4/1) carbonate-rich clay and carbonate-bearing silty clay. Foraminifers are locally abundant in gray (5Y 6/1) calcareous clays. This unit also includes very dark gray (5Y 3/1) silty clay with laminae and beds of silt. The variegated colors are in intervals ranging from 10 to 40 cm thick. Burrow mottling is common to all lithologies. No shipboard carbonate analyses are available from this unit.

Unit VII

Interval: 155-946A-24X-2, 140 cm, through -29X-CC (bottom of hole)
Age: middle Pleistocene
Depth: 220.00 to 273.67 mbsf

The core recovery in Unit VII was less than 19%, and only the top and bottom of this unit were recovered undisturbed (Fig. 2). Unit VII

consists of very dark gray (5Y 3/1) silty clay with numerous laminae and beds of silt (Fig. 12); there is only one thin sand bed. Overall, this unit is similar to the levee sequences cored at other Leg 155 sites.

Mineralogy

Mineralogy was determined by estimation of mineral volume percentages in smear slides and by X-ray diffraction (XRD) analysis.

Smear-slide Synthesis

Carbonate-rich intervals in Unit I (Sample 946A-1H-5, 5–6 cm) and Unit IV (Samples 946A-15H-3, 72–73 cm; -17X-3, 44–45 cm and 104–105 cm; and -24X-1, 145–146 cm) contain about 10%–20% foraminifers and less than 3%–5% terrigenous silt; the remainder is terrigenous clay and calcareous nannofossils. Foraminifer-rich silty clays in Unit IV contain about 15% foraminifers and more than 25% terrigenous silt.

Clay intervals in Subunits IIIA, IIIB, IIIC, and Unit V contain 10%–21% fine silt that consists of about 60% quartz, 15% feldspar, 15% accessory minerals, and 10% plant debris.

Silty sand from a bed rich in clay clasts in Subunit IIIC (Sample 946A-12H-2, 130–131 cm) has a sand:silt:clay ratio of 60:30:10; the sand and coarse silt fraction consists of 64% quartz, 10% feldspar, 10% accessory minerals, 5% mica, 10% foraminifers, and 1% sponge spicules.

XRD Data

Bulk XRD analysis was performed on 19 samples primarily from silty clay intervals in Cores 946A-1H through -29X (Table 2). The common minerals throughout the cored succession, based on the relative intensities of their primary peaks (normalized to quartz intensity), are quartz, plagioclase, augite, and the clay minerals smectite, illite (+ mica), and kaolinite (Fig. 13A, -B). Except for differences in the content of clay minerals, the major mineral groups in silty clay samples show little variation with depth. A few samples contain hornblende and K-feldspar. Sample 946A-7H-2, 123–124 cm, contains siderite.

Spectrophotometry

Light-reflectance values as high as 37% are characteristic of the brown calcareous clay in Unit I, whereas reflectance in the clay, silt, and sand types of Units II to VII ranges between 15% and 25%. Aside from Unit I, only the carbonate-rich intervals in Units IV and VI have reflectance values higher than 25%.

Prominent differences between lithologic units are displayed in the ratio between the red (650–700 nm) and blue (450–500 nm) spectrum reflectance (Fig. 1). The highest red/blue ratio of 1.7 is measured in Unit I and results from the high content of iron oxyhydroxides in the brown calcareous clay. In Units II and III at this site, red/blue ratios associated with silty clays, silt laminae, and silt or sand beds have a mean value of about 1.18, similar to the mean red/blue ratio measured in Units II and III of Site 945. In Units II and III, enhanced red reflectance (red/blue ratio > 1.2) coincides with thick silt and sand beds that contain high amounts of iron-oxide-stained quartz grains. Red/blue ratios slightly lower than 1.18 correspond to core intervals containing silty clay with less abundant silt or sand laminae and beds.

The sediments in Units IV–VII are different in their reflectance character from those above 128 mbsf (Fig. 1). The red/blue ratio in Units IV–VII averages only about 1.1. The lowest values of the red/blue ratio correspond to the carbonate-rich sediments of Units IV and VI. Red/blue ratios below 128 mbsf that exceed 1.1 correspond to core intervals that contain silty clay and silt or sand beds. The distinc-

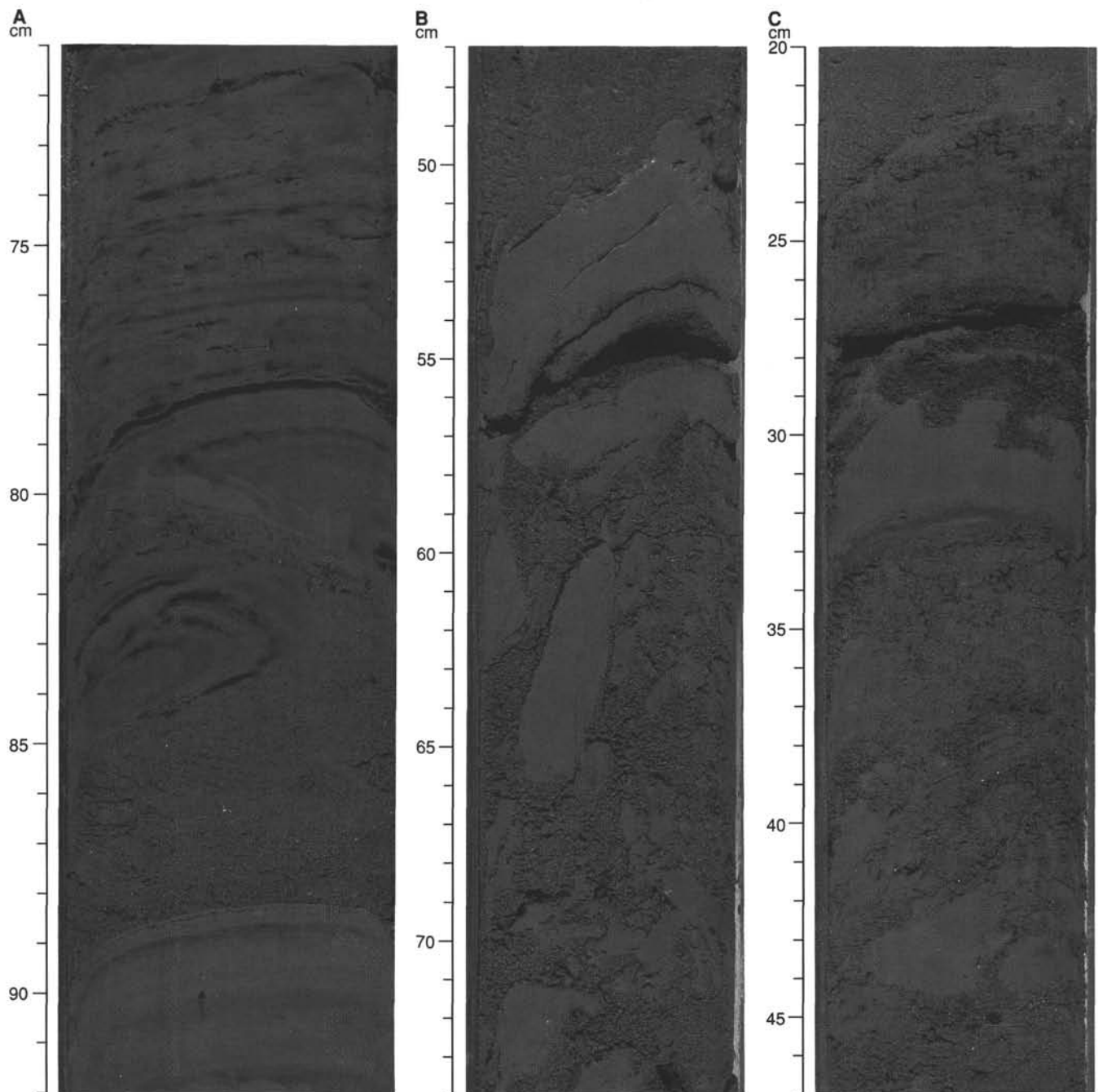


Figure 6. Mud clasts in a sand matrix in Subunit IIIC. **A.** Soft-sediment fold in a color-banded mud clasts (78 to 84 cm). Color-banded clays at 70 to 78 cm and 88 to 94 cm are also probably clasts (155-946A-8H-1, 71–92 cm). **B.** Angular to subrounded mud clasts and mud chips in a matrix of fine sand (155-946A-11H-3, 47–74 cm). **C.** Mud clasts with highly irregular boundaries in a poorly sorted sand matrix that grades upward to silty sand (155-946A-11H-4, 20–47 cm). **D.** Randomly oriented mud clasts in a matrix of poorly sorted, medium to very fine sand; locally, sand matrix has injected some clasts (155-946A-12H-2, 124–150 cm).

tive difference in the red/blue ratio above and below 128 mbsf implies that either the content of iron-oxide-stained quartz grains is generally higher in the sediment above 128 mbsf, or that the sediments in Units IV to VI contain more reduced iron than Units II and III, perhaps because they were deposited more slowly, allowing more complete reduction of iron-bearing phases. Colors determined in Units IV to VI by comparison with Munsell charts tend to be more green than in sediment of Units II and III (e.g., 5GY 4/1 compared with 5Y 4/1), consistent with the presence of more reduced iron.

Discussion

The sediment types from the base of Unit I to 45 mbsf in Hole 946A form two levees of the Amazon Channel System on this part of the fan (see “Setting and Objectives” section, this chapter). These sediment types are similar to levee deposits at other Leg 155 sites except that they contain relatively more silt and sand beds as a result of the lower levee height and greater turbidity-current overspill on this part of the fan.

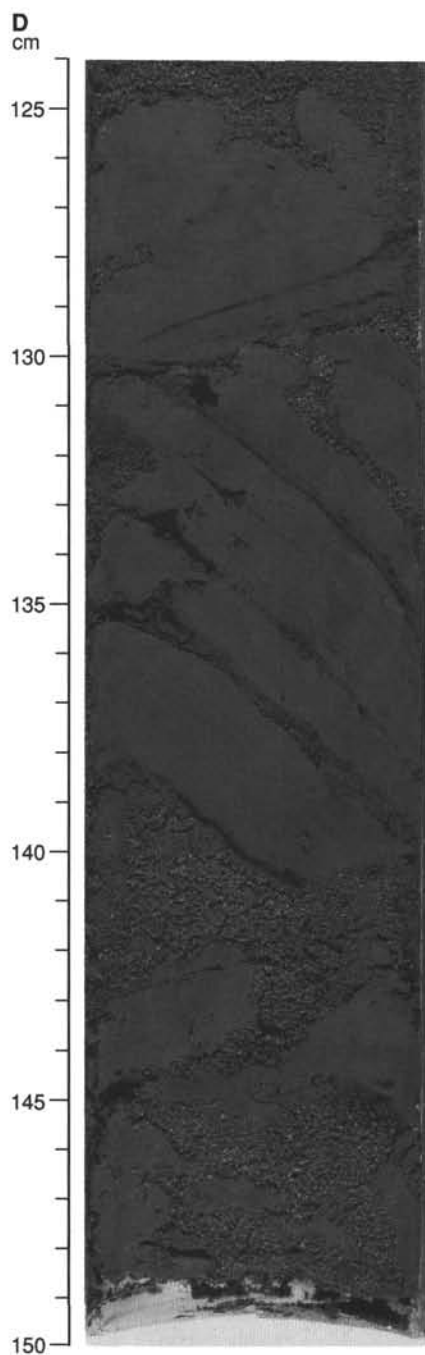


Figure 6 (continued).

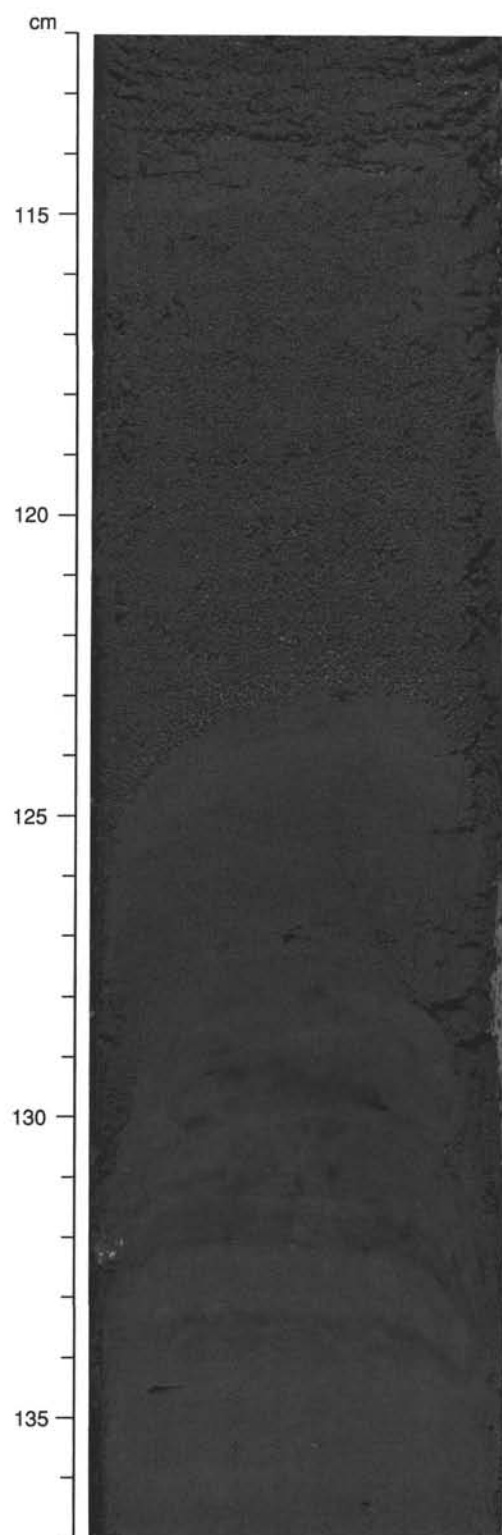


Figure 7. A sharp-based graded sand bed overlying a thin bed of clayey silt (123 to 127.5 cm along core centerline), Subunit IIIC. This clayey silt bed contains subtle cross-lamination (155-946A-13H-2, 112–137 cm).

Sites 945 and 946 are 1.2 km apart. Attempts to correlate sand beds and thin-bedded intervals between the two holes suggest that the deposits of Unit III, below 45 mbsf, have a sheet-like geometry thought to be typical of sand lobes beyond channel terminations. The geometry of these deposits in seismic profiles suggests that they form broad, smooth lower-fan deposits across which the Amazon Channel prograded. Hence, we interpret the interval from 45 to 128 mbsf as deposits of an unconfined sand lobe, now forming a HARP beneath the Amazon Channel. Thick sand beds containing abundant mud clasts may have originated during phases of avulsion and channel-floor downcutting up-fan, similar to the recent phase of downcutting at Site 945. Active downcutting and erosion of the old levee during avulsion may best explain the occurrence of the abundant, semiconsolidated mud clasts and the sand in these deposits.

Most of the sediments recovered from Units IV through VII are muddy, including some intervals that are carbonate-rich and moderately to intensely burrowed. The carbonate-rich intervals presumably correspond to times of elevated sea level and trapping of Amazon River sediment in nearshore or inner-shelf environments. Downhole logs, however, indicate that much of the sediment in intervals of little

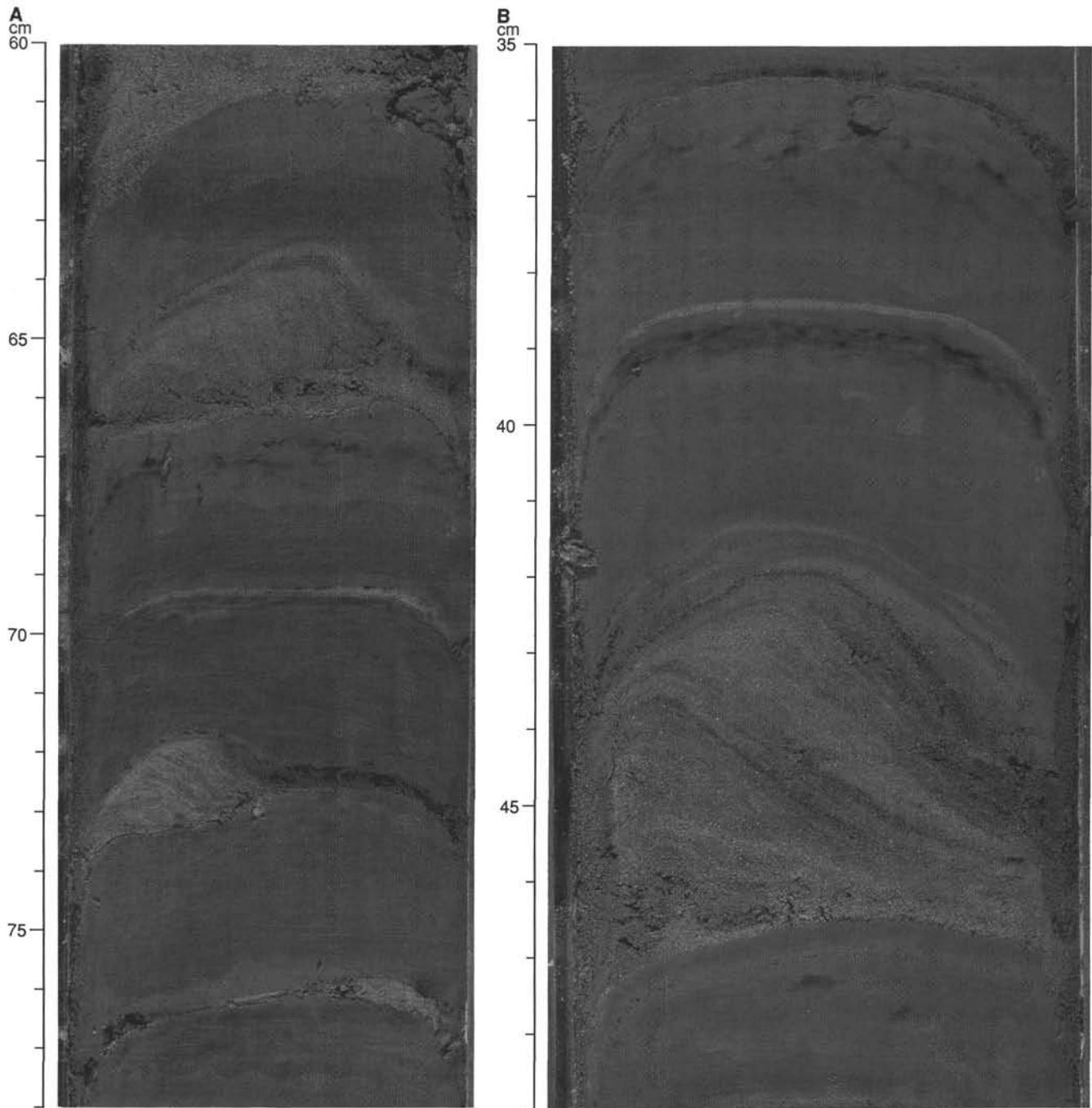


Figure 8. Silty clay with wavy bedded, cross-laminated silt and silty sand beds in Subunit IIIC. **A.** 155-946A-13H-4, 60–78 cm. **B.** 155-946A-13H-4, 35–49 cm. Note that the very fine silty sand bed (42–47 cm) passes gradationally upward, through a division of alternating silt/mud laminae, into the overlying mud (39–42 cm) and therefore represents a T_{cde} turbidite.

or no recovery is thickly bedded sand, similar in sand-mud ratio to parts of Subunit IIIC. Some of this sand was recovered in Cores 946A-21X and -23X, possibly because abundant mud clasts at this stratigraphic level kept sand from falling out of the core barrel. These mud-clast-rich deposits are similar to the thicker beds in Subunit IIIC, and perhaps were also formed as a consequence of avulsion-related downcutting into older deposits up-fan from Site 946. If true, then the unifying theme of Site 946 (and Site 945) might be cycles of (1) deposition of sand lobes rich in mud clasts down-fan from the terminations of young channel segments following up-fan avulsion, and (2) progradation of muddy levees across the sheet-like sandy lobes.

Because the recovery below 160 mbsf is so poor, evaluation of any cyclicity between HARP sand sheets (i.e., sand lobes) and levee deposits must be based on the interpretation of logging data, particularly FMS logs (see “Downhole Logging” section, this chapter).

BIOSTRATIGRAPHY Calcareous Nannofossils

An abundant and well-preserved nannofossil assemblage with high diversity is present in the calcareous nannofossil and foraminifer

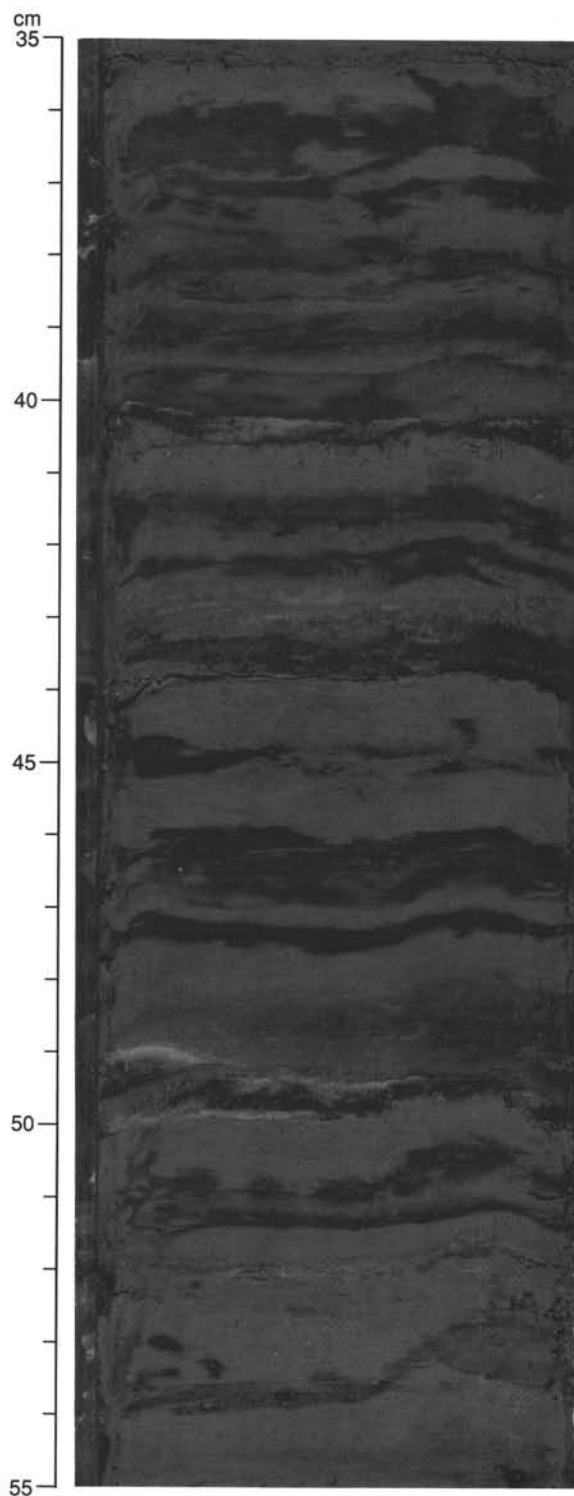


Figure 9. Black bands in a moderately burrowed silty clay that contains burrow-disrupted silt laminae, Unit IV (155-946A-16X-6, 35–55 cm).

clay (Unit I) in the mud-line sample (Table 3). This assemblage includes a number of species of the genera *Helicosphaera* and *Thoracosphaera*. Nannofossils are rare or absent in Units II and III to a depth of 117 mbsf (Samples 946A-1H-CC, 14–15 cm, through -13H-CC, 0 cm). The lack of nannofossils in these units may be due to a shallower calcium compensation depth (CCD) in the Atlantic Ocean during the glacial periods, which would have had a significant influ-

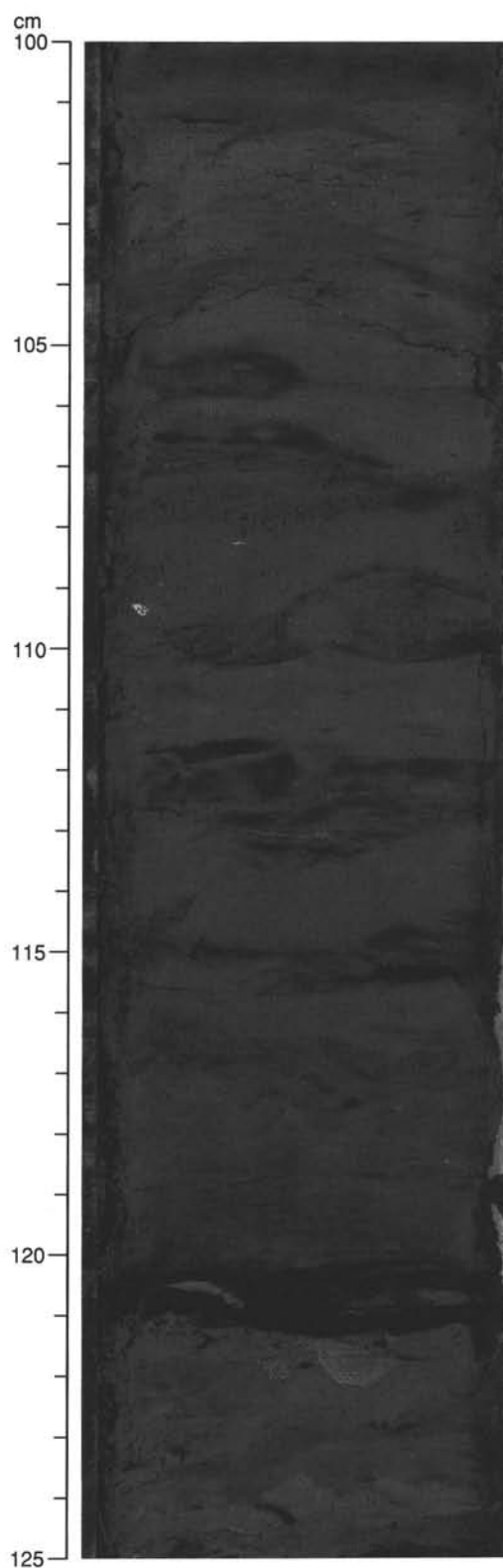


Figure 10. Contrasting colors of darker silty clay and lighter carbonate-rich clay in Unit IV (155-946A-17X-3, 100–125 cm). Scattered foraminifera are present on the core surface from 102 to 106 cm.

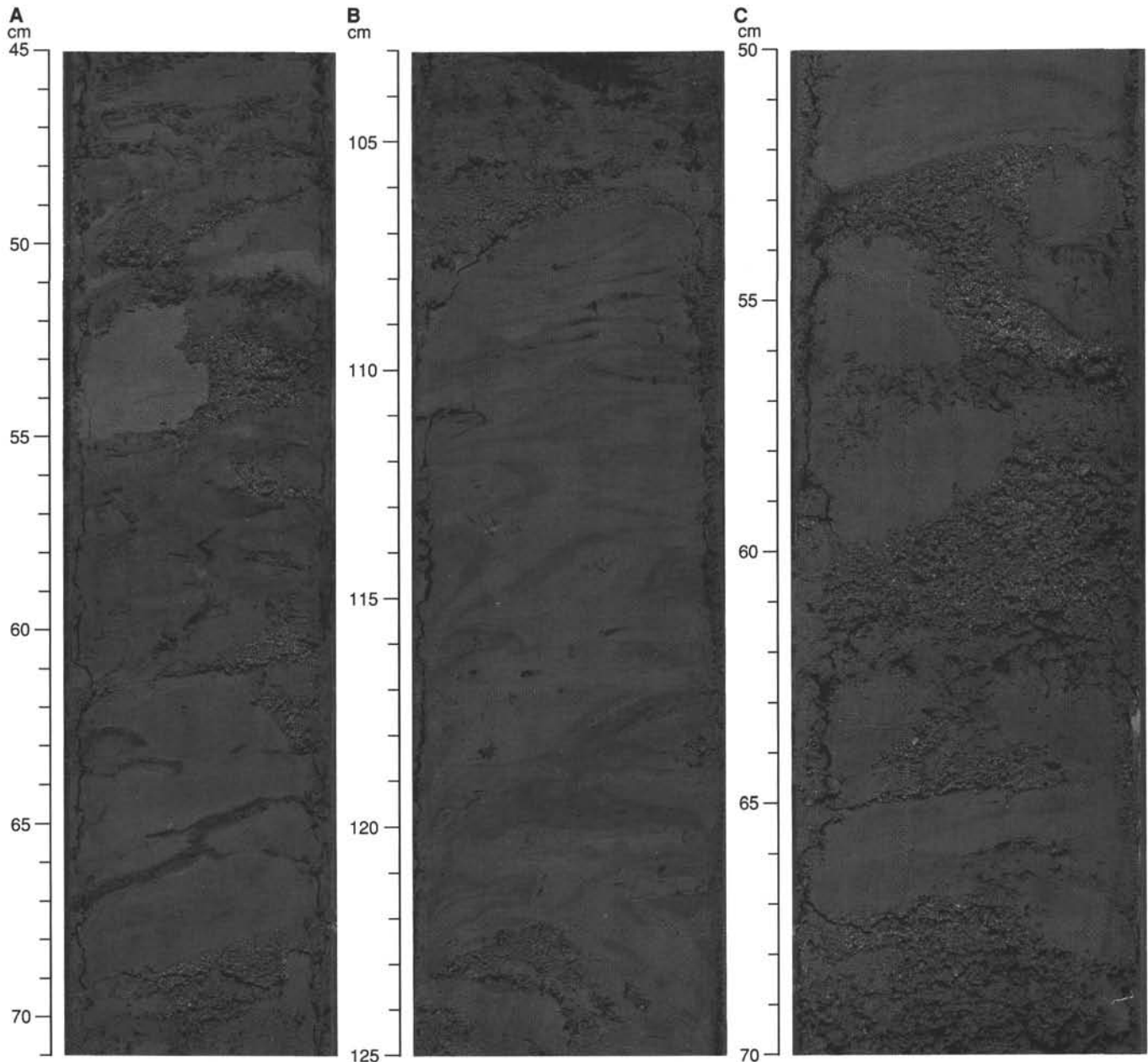


Figure 11. Mud clasts in a matrix of medium to coarse sand, Unit V. **A.** Angular light-colored carbonate-rich clasts and silty clay clasts (155-946A-21X-1, 45–71 cm). **B.** Internally folded clast(s) with a “wood-grain” fabric produced by drilling-biscuit formation during rotary coring with the XCB system (155-946A-21X-1, 103–125 cm). **C.** Irregularly shaped clasts in a poorly sorted sand matrix (155-946A-21X-3, 50–70 cm).

ence at the water depth of this site. A number of light-colored clasts within Subunit IIIC at 57.2 and 96.6 mbsf contained authigenic carbonate minerals (siderite) and were barren of nannofossils (Samples 946A-7H-2, 123–124 cm, and -11H-3, 110–112 cm).

Unit IV (Sample 946A-14H-6, 90 cm) contains a fairly diverse nannofossil assemblage including large-sized *Gephyrocapsa* specimens, small *Reticulofenestra* species, and *E. huxleyi*, placing the unit in Zone CN15a. Samples across a carbonate-rich interval within Core 946A-15H at 133 mbsf (Samples 946A-15H-3, 60 cm, 66 cm, 77 cm) show high abundances of nannofossils with diverse and well-preserved nannofloras of Zone CN15a, including species of *Pontosphaera* and *Thoracosphaera*. Reworked Miocene discoasters were observed in Sample 946A-15H-3, 66 cm. The abundance of nanno-

fossils varies throughout Core 946A-15H from 130 to 137 mbsf from abundant to very rare in intervals dominated by silt-sized (10–20 μm) angular to sub-rounded quartz grains. An interval of rare and poorly preserved nannofossils occur from 143.3 mbsf to 147.71 mbsf (Samples 946A-16X-3, 33–34 cm, through -16X-6, 33–34 cm). The abundance of nannofossils also varies greatly from 149.6 to 154.2 mbsf throughout Core 946A-17X. The lower part of Section 946A-17X-5 and Section 946A-17X-6 is barren of nannofossils.

In Unit V from 155 to 211 mbsf, a light-colored clast within a homogenous and nonfossiliferous clay contained a rich nannofossil assemblage dominated by *Gephyrocapsa* sp. (Sample 946A-21X-1, 53 cm). This assemblage is similar to the underlying assemblages of the hemipelagic Unit VI. Closely spaced samples from a carbonate-rich

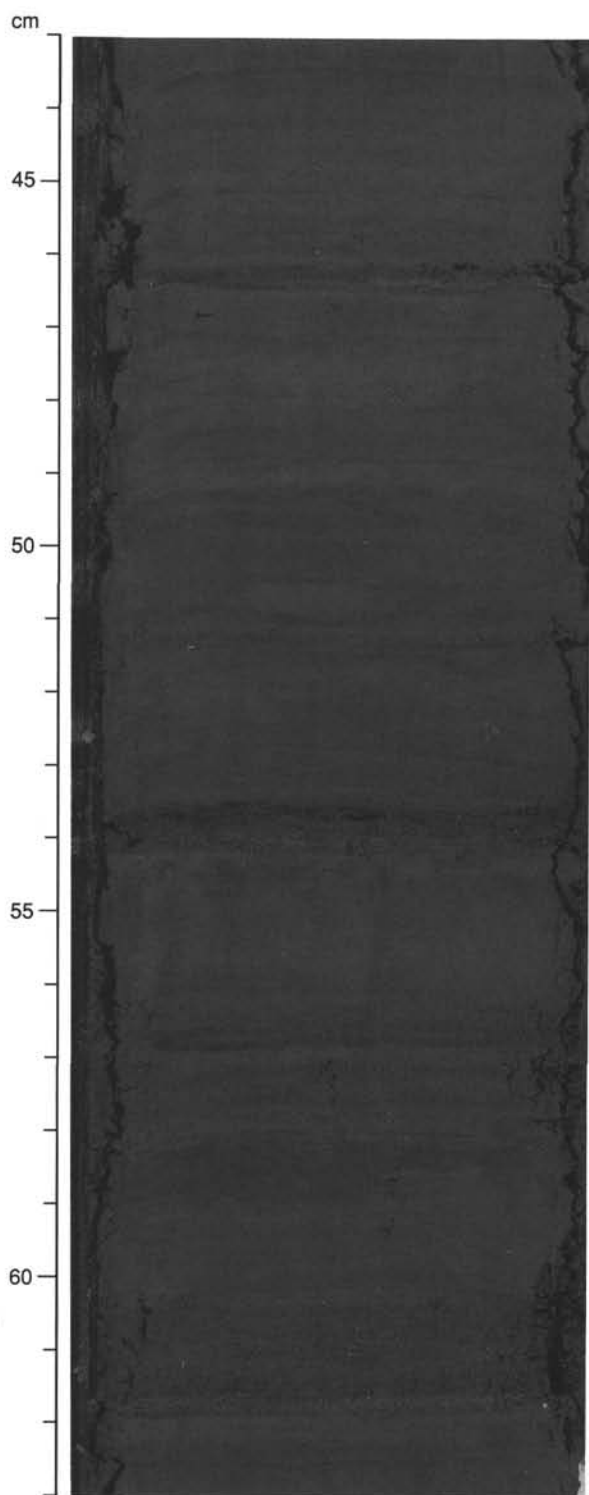


Figure 12. Thin-bedded couplets of silt and laminated silty clay from the levee sediment of Unit VII (155-946A-29X-5, 43–63 cm).

interval of Unit VI (e.g., Sample 946A-23X-4, 10 cm) provide a well-preserved, highstand nannofossil assemblage dominated by *Gephyrocapsa* sp. The assemblages are lacking *P. lacunosa* and *E. huxleyi* and are thus constrained in age between 0.26 and 0.46 Ma (Zone CN14b). The *Gephyrocapsa* sp. assemblages resemble the nannofloras found in the deep carbonate units of Sites 931, 933, and possibly those at Sites 935 and 936. A sample scraped from the split surface

from 197.8 mbsf (Section 946A-22X-CC) contained poorly preserved nannoflora including the cold-water species *C. pelagicus*. The nannoflora of Unit VII from 220 mbsf to 273 mbsf (Samples 946A-24X-CC, 12–13 cm, through -29X-CC, 9–18 cm) is a rare and poorly preserved glacial flora.

Planktonic Foraminifers

The boundary between Ericson Zones Z and Y is between 7.04 mbsf (Sample 946A-1H-CC, 5 cm) and 16.30 mbsf (Sample 946A-2H-CC, 5 cm; Table 4 and Fig. 14) based on the disappearance of *G. tumida*. However, given the possible downhole contamination of the core-catcher samples, the Z/Y boundary is most likely associated with the base of Unit I.

Unit III from 16.3 to 117.4 mbsf has been defined as the Y Zone due to the absence of *G. tumida* (Samples 946A-2H-CC, 5 cm, through -13H-CC, 0 cm). Unit III contains an extremely low abundance of planktonic foraminifers (some of which are iron stained) as well as mica, fine organics, leaves, wood, and sand, indicating a reworked component. Unit IV and the top of Unit V from 130.5 to 168.9 mbsf have been defined as the interglacial Ericson X Zone (generally equivalent to oxygen isotopic Stage 5) due to the presence of *G. tumida* (Samples 946A-15H-1, 15 cm, through -19X-CC, 10 cm). Foraminifers are abundant and well preserved in Unit IV with no indicators of reworking. Authigenic black nodules occur in Unit IV and the top of Unit V. Poor recovery from 159 to 256 mbsf in Units V through VII makes biostratigraphic interpretation difficult. Unit V contains sand, wood, mica, black nodules, and pteropods, suggesting reworking. Planktonic foraminifers are absent from sediment recovered from the bottom of Unit V. A second carbonate-rich layer in Unit VI from 211 to 218.7 mbsf contains abundant interglacial foraminifers, including *G. tumida* and *G. menardii* (946A-23X-3, 50 cm, through -24X-2, 13 cm). This interval has been initially interpreted as the Ericson Zone V. However, the low abundance of foraminifers and the poor recovery (22%) makes identification of iterative "Ericson zone" biostratigraphy difficult. If this interpretation is correct, then the majority of Unit V is Ericson Zone W and Unit VII is Zone U.

Benthic Foraminifers

Benthic foraminifers are rare to absent in Hole 946A.

Siliceous Microfossils

Marine diatoms were observed in low abundance only in the mudline sample of Hole 946A.

Palynology

Six samples were examined from Hole 946A (Table 5). The late Pleistocene (Y Zone) pollen and spore assemblages in Unit III from 7.04 to 74 mbsf (946A-1H-CC, 14–15 cm, through -8H-CC, 14–15 cm) have relatively high abundances and good preservation. The assemblage includes Proteaceae, *Cecropia*, Gramineae, TCP (tricolpate) and TC (tricolpate) pollen types, with Grammatidaceae, Cyatheaceae, trilete, and monolet spores. Good preservation suggests that older reworked spores do not make a significant contribution to the total palynomorph assemblage in this unit. Two samples at 117.4 and 131.8 mbsf (946A-13H-CC, 0 cm, and -14H-CC, 26–27 cm) have low abundance and moderate preservation, with tricolpate (TCP) pollen type and Cyatheaceae spores present. Wood particles were observed in all sample slides in moderate to high abundance. Macroscopic wood (>63 μ m), including intact seeds and leaf material, was observed in the core-catcher samples at 82.78 mbsf, 85.60 mbsf, and 160.81 mbsf (Table 5). Dinoflagellates are not present.

Table 2. Relative peak intensities of main minerals in representative samples for most cores recovered at Site 946.

Core, section, interval (cm)	Lithology	Depth (mbsf)	Relative intensity of primary peaks									
			Smectite	Mica + Illite	Kaolinite	Quartz	Plagioclase	K-feldspar	Augite	Hornblende	Calcite	
155-946A-												
1H-3, 72-73	Silty clay	3.72	12.5	21.0	16.3	100.0	6.3	*	3.3	*	*	
2H-2, 19-20	Silty clay	8.74	5.1	17.3	9.1	100.0	10.2	4.7	1.9	1.1	*	
3H-4, 30-31	Silt	21.30	6.8	12.5	5.0	100.0	10.5	5.1	1.9	*	*	
4H-5, 88-89	Silty clay	32.78	6.2	15.9	9.4	100.0	7.4	3.8	2.5	*	*	
5H-2, 128-129	Silty clay	38.28	6.5	18.7	10.3	100.0	7.8	5.9	2.7	*	*	
7H-2, 123-124	Carbonate-rich clast	57.23	*	10.7	4.6	100.0	7.2	*	*	*	*	
8H-5, 140-141	Silty clay	71.40	6.9	15.0	7.7	100.0	9.8	*	2.2	*	*	
9H-4, 58-59	Silty clay	78.58	6.5	16.3	9.7	100.0	9.3	*	2.9	*	*	
10H-1, 118-119	Silty clay	84.18	8.9	21.6	8.5	100.0	7.9	*	3.3	1.3	*	
11H-4, 98-99	Silt	97.98	10.8	17.0	10.6	100.0	*	6.9	3.2	*	*	
12H-3, 93-94	Sand	105.93	6.3	19.3	9.4	100.0	8.6	*	3.0	*	*	
13H-4, 29-30	Silty clay	116.29	11.0	19.8	7.6	100.0	8.8	5.4	2.5	*	*	
14H-7, 97-98	Silty clay	130.50	3.6	13.0	7.5	100.0	6.3	*	*	*	7.0	
16X-2, 76-77	Carbonate-bearing clay	142.26	9.3	15.5	10.9	100.0	8.3	*	*	*	13.3	
17X-4, 17-18	Carbonate-bearing clay	154.27	*	17.4	12.1	100.0	9.0	*	*	*	*	
18X-1, 9-10	Silty clay	159.29	4.3	18.6	10.2	100.0	7.3	*	2.4	*	*	
21X-3, 15-16	Sand	191.35	5.3	16.0	10.5	100.0	8.8	*	3.0	*	*	
24X-3, 44-45	Sand	220.54	*	2.4	0.8	100.0	5.8	3.6	0.6	2.2	0.6	
29X-5, 73-74	Silty clay	272.13	11.3	29.1	16.0	100.0	10.4	5.2	2.4	*	*	

Notes: See "Lithostratigraphy" section in the "Explanatory Notes" chapter, this volume, for XRD methods. * = non-detection.

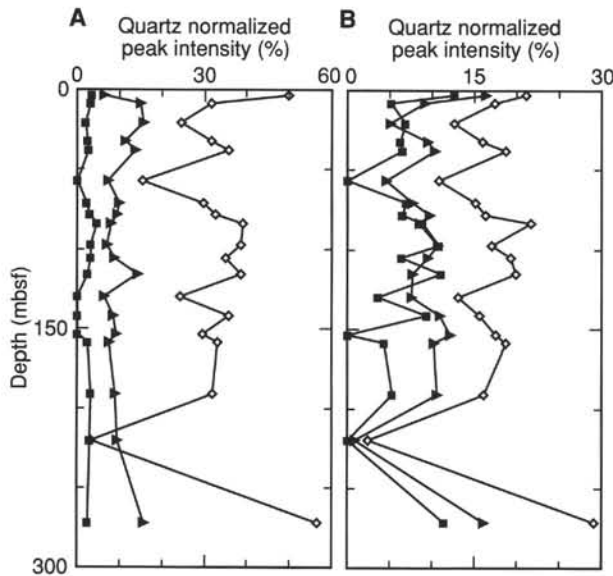


Figure 13. Relative abundances of silicate minerals in representative samples, based on XRD analysis (Table 2). **A.** Downhole variation in the relative peak intensities of the main mineral groups. Diamonds = clay minerals + mica; triangles = feldspar; squares = augite + hornblende. **B.** Downhole variation in the relative peak intensities of clay minerals and micas. Squares = smectite; diamonds = mica + illite; triangles = kaolinite.

Stratigraphic Summary

Unit I contains well-preserved planktonic foraminifer assemblages indicative of the Holocene. The nannofossil assemblage in Unit I represents nannofossil Zone CN15b.

The Ericson Zone Z/Y boundary is most likely located at the base of Unit I above the first core-catcher sample at 7.04 mbsf, given probable downhole contamination of the core catcher. Subunits IIIB and IIIC have been defined as the Y Zone due to the absence of *G. tumida*. This Ericson Zone age assignment is supported by the identification of the paleomagnetic Lake Mungo Excursion (30 ka) at 103 mbsf. The 40-ka *Y_{p. obliq.}* datum is not observed before the X Zone fauna is encountered in Unit IV. Unit IV and the top of Unit V have been defined as the interglacial X Zone due to the presence of *G. tumida*. This is supported by the identification of the paleomagnetic Blake Event (105 ka) at 133 mbsf. The nannofossil data indicate Zone

CN15a (0.085–0.26 Ma). The carbonate-rich interval in Unit VI from 211 to 218.7 mbsf contains abundant interglacial foraminifers, including *G. tumida* and *G. menardii*. The nannofossil assemblage in Unit VI represents Zone CN14b and is dominated by *Gephyrocapsa*. This indicates that there is not a continuous sequence of Ericson foraminifer zones recovered in the hole.

PALEOMAGNETISM

Remanence Studies

Archive-half core sections from 13 APC cores and seven XCB cores were measured. Cores 946A-6H and -10H, which were entirely composed of sand, were not measured. The Tensor tool was used to orient Cores 946A-3H through -8H and Cores 946A-11H through -15H.

Oscillations in declination and inclination, interpreted as secular variation, were best developed in Core 946A-2H (Fig. 15). Their wavelength was ~0.25 m in this 3-m interval.

Remanence intensity, after AF demagnetization to 20 mT, showed considerable variability in Hole 946A, with the highest average values from 0 to 10 mbsf, and the greatest range of intensities between 125 and 200 mbsf in lithostratigraphic Units IV and V (Fig. 16). From 0 to 50 mbsf, three peaks in remanence intensity are seen. These peaks have a pattern similar to that of the intensity peaks identified in other Amazon levee sites (see Fig. 15 of "Site 940" chapter, this volume).

Two anomalous intervals of remanence direction and intensity that may represent geomagnetic excursions appeared in Hole 946A. The first occurred in Section 11H-7 (101.5–101.8 mbsf) and consisted of a short interval of moderately high positive inclinations (>40°) accompanied by a doubling of remanence intensity. The second was coincident with a carbonate zone in Section 15H-3 (133.2–134.0 mbsf) and was characterized by a shift to high positive inclinations and a weakening of remanence intensity (Fig. 17). Because of the character of the remanence behavior of these two intervals, we interpret the first as the Lake Mungo Excursion (~30 ka) and the second as the Blake Event (~105 ka).

Magnetic Susceptibility Studies

Whole-core magnetic and discrete-sample susceptibilities were measured on all cores collected from Site 946. Both data sets show similar downhole trends (Fig. 18).

The lowest values are within the carbonate units: Units I, IV, and VI. This reflects the dilution of the magnetic minerals by biogenic

Table 3. Calcareous nannofossil and siliceous microfossil abundance data for Hole 946A.

Core, section, interval (cm)	Top interval (mbsf)	Bottom interval (mbsf)	Calcareous nannofossils			Diatoms		Sponge spicules	Radiolarians	Ericson Zone (inferred from foraminifers)	Age (inferred from foraminifers)
			Abundance	Preservation	Zone	Marine	Freshwater				
155-946A-											
1H-MI, 0	0.00		a	g	CN15b	—	—	—	—	Z	Holocene
1H-1, 0-1	0.00	0.01	a	g		—	—	—	—		
1H-CC, 14-15	7.04	7.05	b	—		—	—	—	—		
2H-CC, 4-5	16.29	16.30	b	—		—	—	—	—	Y	late Pleist.
3H-CC, 11-12	26.29	26.30	tr	—		—	—	—	—		
4H-CC, 27-28	35.85	35.85	b	—		—	—	—	—		
5H-CC, 59-60	45.36	45.37	b	—		—	—	—	—		
6H-CC, 49-50	53.59	53.60	b	—		—	—	—	—		
7H-2, 123-124	57.23	57.24	b	—		—	—	—	—		
7H-CC, 8-9	64.04	64.05	b	—		—	—	—	—		
8H-CC, 14-15	74.00	74.01	b	—		—	—	—	—		
9H-CC, 4-5	82.82	82.83	b	—		—	—	—	—		
10H-CC, 4-5	85.64	85.65	b	—		—	—	—	—		
11H-3, 110-112	96.60	96.62	b	—		—	—	—	—		
12H-CC, 40-41	110.05	110.06	b	—		—	—	—	—		
13H-CC, 0	117.40		b	—		—	—	—	—		
14H-6, 90	128.93		f	—	CN15b?	—	—	—	—		
14H-CC, 26-27	131.84	131.85	r	m		—	—	—	—		
15H-1, 15	130.65		c	m	CN15a	—	—	—	—	X	late Pleist.
15H-1, 68	131.18		b	—		—	—	—	—		
15H-1, 140	131.90		r	g		—	—	—	—		
15H-2, 7	132.05		tr	m		—	—	—	—		
15H-2, 67	132.65		b	—		—	—	—	—		
15H-3, 3	132.90		c	m		—	—	—	—		
15H-3, 20	133.07		a	m		—	—	—	—		
15H-3, 45	133.32		f	p		—	—	—	—		
15H-3, 56	132.43		c	g		—	—	—	—		
15H-3, 60	133.03		a	m		—	—	—	—		
15H-3, 66	133.09		a	g		—	—	—	—		
15H-3, 77	133.20		a	m		—	—	—	—		
15H-3, 83	133.26		f	m		—	—	—	—		
15H-3, 97	133.40		vr	—		—	—	—	—		
15H-3, 109	133.52		r	p		—	—	—	—		
15H-4, 38	134.75		f	p		—	—	—	—		
15H-4, 117	135.54		r	—		—	—	—	—		
15H-5, 38	136.25		f	m		—	—	—	—		
15H-CC, 21-22	137.51	137.52	vr	p		—	—	—	—		
16X-CC, 40-41	149.35	149.36	c	g	CN14b	—	—	—	—		
17X-CC, 78-79	159.35	159.36	b	—		—	—	—	—		
18X-CC, 20-21	160.90	160.91	b	—		—	—	—	—	?W	middle Pleist.
19X-CC, 10-11	168.90	168.91	tr	—		—	—	—	—		
21X-1, 53	188.73		a	g		—	—	—	—		
21X-CC, 29-30	193.29	193.30	f	p		—	—	—	—		
22X-CC, 2-3	197.82	197.83	f	p		—	—	—	—		
23X-3, 58-59	211.08	211.09	b	—		—	—	—	—	?V	middle Pleist.
23X-4, 10-11	212.10	212.11	c	m		—	—	—	—		
23X-CC, 19-20	212.35	212.36	r	—		—	—	—	—		
24X-1, 59-60	217.69	217.71	vr	p		—	—	—	—		
24X-2, 113-14	218.73	218.74	a	g		—	—	—	—		
24X-CC, 12-13	221.72	221.73	vr	—		—	—	—	—	?U	middle Pleist.
28X-CC, 12-21	256.04	256.05	tr	—		—	—	—	—		
29X-3, 45-46	248.85	248.86	vr	—		—	—	—	—		
29X-CC, 9-18	273.57	273.66	b	—		—	—	—	—		

material. The highest values are within the coarse-grained units, in particular, Subunit IIIc. The sharp drop in whole-core susceptibility at 128 mbsf corresponds to a decrease in the red/blue reflectance ratio as measured by the color scanner (Fig. 1).

ORGANIC GEOCHEMISTRY

Volatile Hydrocarbons

Headspace methane concentrations increase rapidly below the sediment surface to a maximum value of 14,400 ppm at 11.55 mbsf (Table 6; Fig. 19). Below this depth headspace methane concentrations remain fairly constant, ranging from 4400 ppm to 13,100 ppm. Vacutainer methane values are considerably higher than headspace concentrations (Fig. 19), ranging from 26,000 ppm at 41.50 mbsf to ~520,000 ppm at ~132 mbsf. Higher molecular weight hydrocarbons were not measured, indicating a predominantly biogenic methane source at Site 942.

Carbon, Nitrogen, and Sulfur Concentrations

This report includes elemental data of samples from the first 17 cores of Hole 946A to a depth of 159.22 mbsf. Analyses of samples from the rest of the hole will be done post-cruise.

Carbonate (calculated as CaCO₃) concentrations are generally low (<4.0%) between 0.68 and 106.29 mbsf (Table 7; Fig. 20) within lithologic Units II and III. One high carbonate value (12.8%) was measured at 55.40 mbsf in a sample of gray (5GY 4/1) clay. Several samples with high carbonate content, ranging from 6% to 36%, were found between 130.94 and 153.04 mbsf in lithologic Unit IV. The carbonate concentration profile shows three discrete maxima, at 133.31 mbsf (18.3%), 144.27 mbsf (32.2%), and at 148.55 mbsf (35.5%). Below Unit IV, the carbonate content decreases to 3.6% at 159.22 mbsf.

TOC values range between 0.8% and 1.3% in samples of lithologic Units II and III. A high value of 4.1% is obtained from a silty clay sample with abundant plant debris at 42.13 mbsf. Samples of Unit IV are characterized by lower TOC values ranging from 0.3% to 0.6%. All samples with carbonate values >18% have TOC concentrations ≤0.4%. Below Unit IV the TOC increases to ~0.9% at 159.22 mbsf.

Total nitrogen concentrations at this site show a profile similar to that of TOC. The values range between 0.08% and 0.15% with lower values (0.08%–0.11%) in lithologic Unit IV. The highest value (0.15%) corresponds to the sample at 42.13 mbsf, which is rich in plant debris. Total sulfur concentrations are low (<0.15%) throughout Site 946. The [C/N]_a ratios in Units II and III generally range from 7 to 13, except for a high value (32) in the plant-debris-rich sample at 42.13 mbsf. This value is typical for terrestrial organic matter.

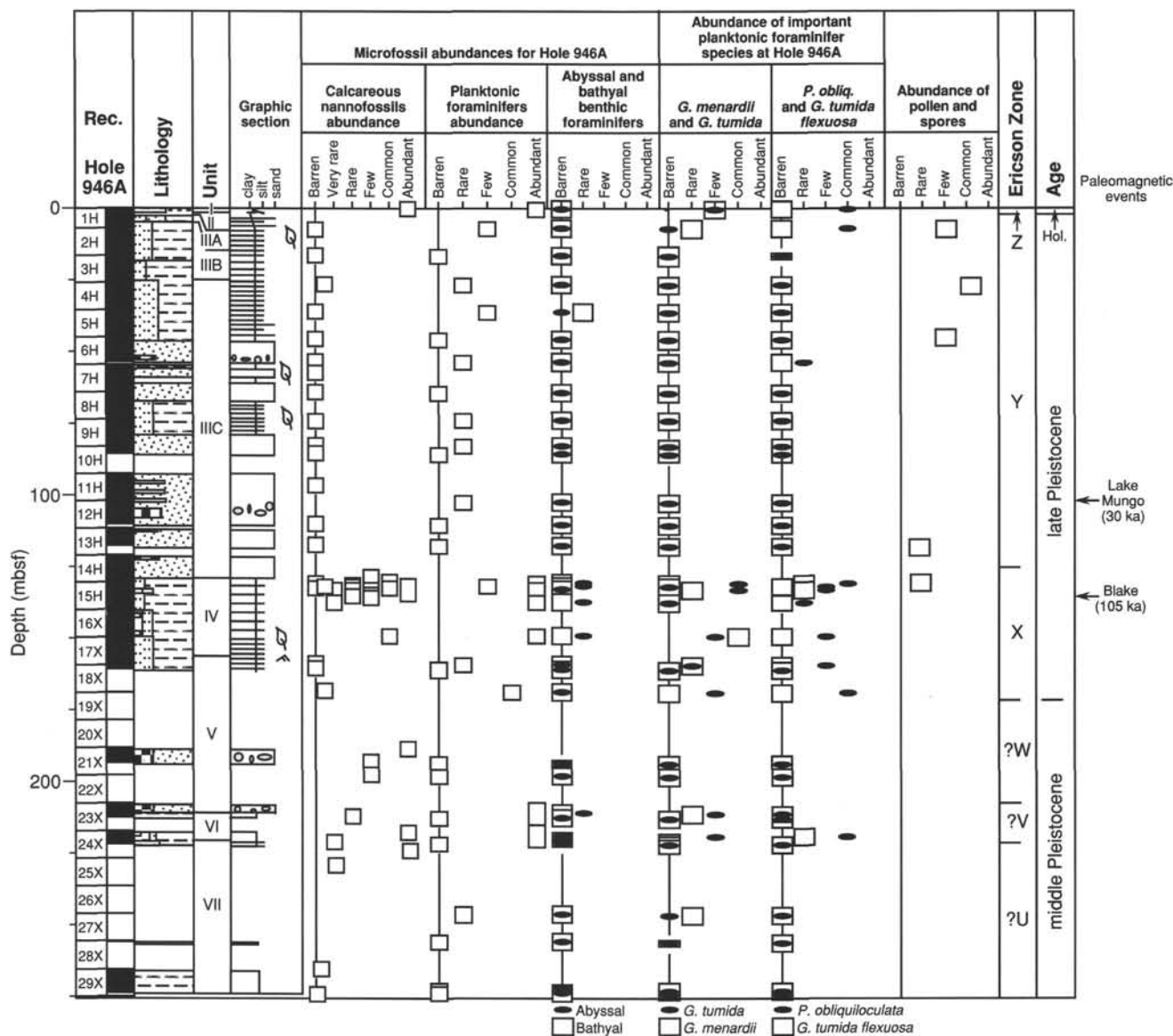


Figure 14. Biostratigraphic summary for Site 946.

Significantly lower [C/N]_a ratios (4–7) were observed in lithologic Unit IV, suggesting a higher portion of marine-derived organic matter compared to other samples from Hole 946A.

The interval between 130.94 and 153.04 mbsf, which represents Ericson Zone X, is characterized by an elemental composition differ-

ent from that of the rest of Site 946. This interval shows three peaks of high carbonate content that probably represent hemipelagic deposition during sea level highstands. The TOC concentrations in this interval are similar to those of Holocene sediment at previous sites and the deeper carbonate-rich interval encountered at Site 942.

Table 5. Spores and pollen data for Hole 946A.

Core, section, interval (cm)	Top interval (mbsf)	Bottom interval (mbsf)	Pollen and spores		Major types recorded	Dinocysts	Wood/carbonized particles	Ericson Zone (inferred from forams.)	Age (inferred from forams.)
			Abundance	Preservation					
155-946A-1H-CC, 14–15	7.04	7.05	f	g	Cyatheaceae, tricolporate, trilete spores	b	c	Z	Holocene
3H-CC, 11–12	26.29	26.30	c	m	Proteaceae, Cyatheaceae, Grammatidaceae (?), monolete spore	b	f	Y	late Pleist.
5H-CC, 59–60	45.36	45.37	f	m	Cyatheaceae, tricolporate	b	f	Y	late Pleist.
8H-CC, 14–15	74.00	74.01	c	m	Gramineae, Cyatheaceae, tricolporate, monolete spore (scabrata), <i>Cecropia</i>	b	a	Y	late Pleist.
13H-CC, 0	117.40		r	m	Tricolporate	b	c	Y	late Pleist.
14H-CC, 26–27	131.84	131.85	r	m	Cyatheaceae	b	f	Y	late Pleist.

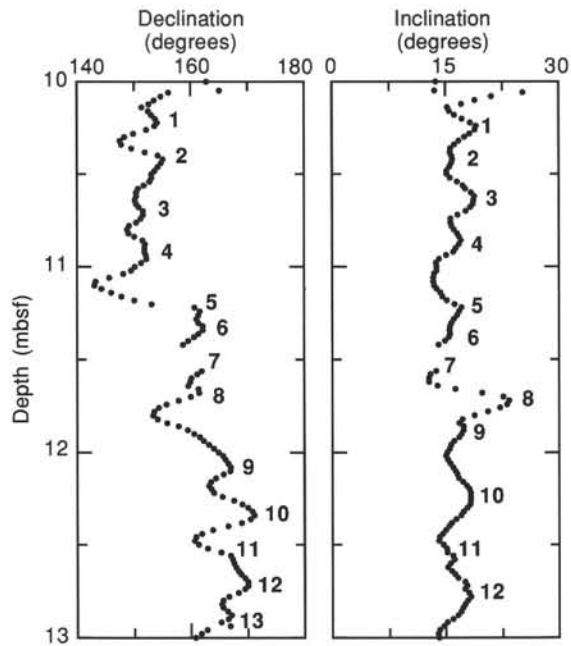


Figure 15. Uncorrected declination and inclination, after AF demagnetization to 20 mT, for a 3-m interval of Hole 946A. Oscillations interpreted as secular variation cycles are numbered sequentially.

INORGANIC GEOCHEMISTRY Interstitial Water Analysis

Interstitial water samples were collected from 13 sediment samples from Hole 946A (Table 8; Fig. 21). Samples were taken at approximately 10-m intervals for the first 40 m and approximately every 30 m thereafter. In addition, two samples were taken from rapidly degassing sand layers in Core 946A-9H. Poor recovery prevented sampling between 131.88 and 191.10 mbsf.

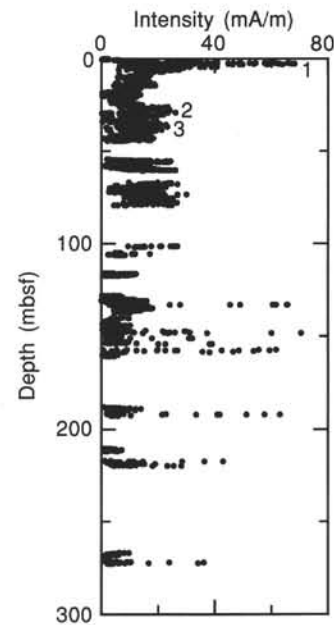


Figure 16. Remanence intensity, after AF demagnetization to 20 mT, for Hole 946A. Intensity peaks are numbered 1–3.

Salinities of the water samples decrease from 34.0 at 1.45 mbsf to 32.0 at 11.50 mbsf (Fig. 21A). The salinity increases slightly to 33.0 at 72.95 mbsf, then decreases again to 32.0 at 106.40 mbsf, and remains at 32.0 through the remainder of the hole. Chloride concentrations increase gradually from 552 mM at 1.45 mbsf to 565 mM at 82.45 mbsf (Fig. 21B). The concentrations then decrease sharply to 549 mM between 106.4 and 131.88 mbsf and remain at approximately 545 mM for the remainder of the hole. The two samples from Core 946A-9H were taken to evaluate the possible presence of gas hydrates, but no change in chloride concentration was observed. Pore-water pH generally ranges from 7.49 to 7.70 (Fig. 21C), except for a pH of 7.92 at 131.88 mbsf. There is no clear trend downhole. The

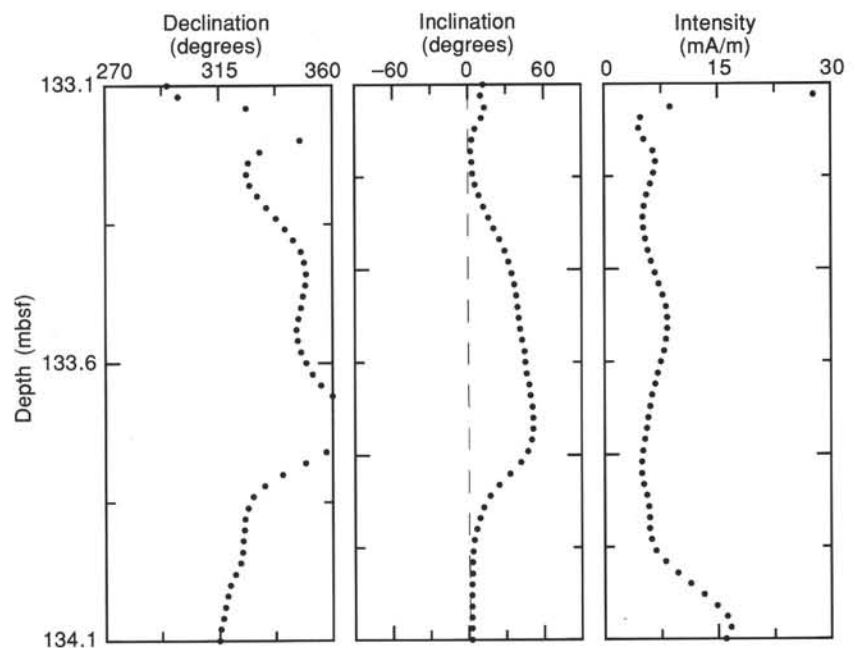


Figure 17. Uncorrected declination, inclination, and remanence intensity, after AF demagnetization to 20 mT, for a 1-m interval of Section 155-946A-15H-3, which may have recorded the Blake Event (105 ka).

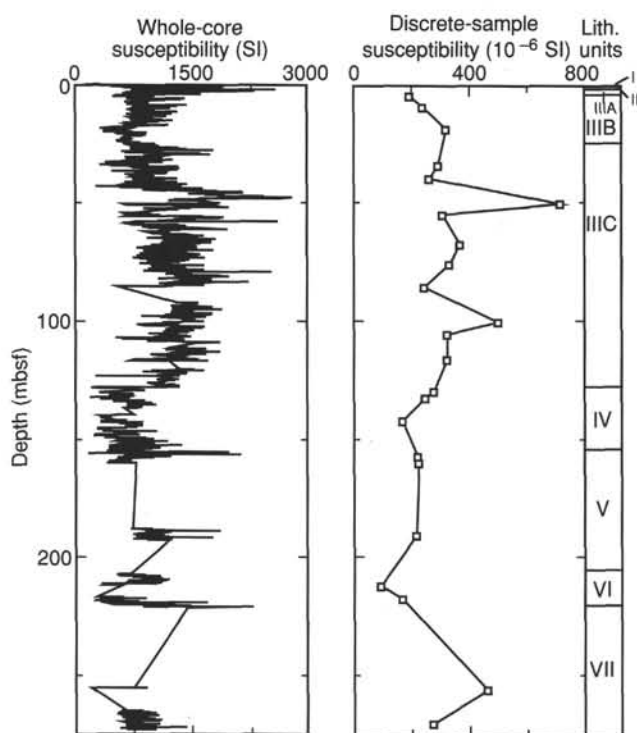


Figure 18. Whole-core and discrete-sample susceptibility for Hole 946A.

pore-water alkalinity profile (Fig. 21D) is similar to that for pH. Concentrations fall between 9.58 and 13.78 mM with the exception of the sample taken at 131.88 mbsf, which has an alkalinity of 26.28 mM. This sample is near a carbonate-rich layer (see "Lithostratigraphy" section, this chapter), possibly explaining the high pH and alkalinity.

Dissolved magnesium concentrations decrease from 51.0 to 42.5 mM between 1.45 and 11.50 mbsf (Fig. 21E). The concentrations increase slightly to around 45 mM at 23.95 mbsf, and remain at that level through 106.40 mbsf. Concentrations then decrease gradually to

Table 6. Gas concentrations in sediments from Site 946.

Core, section, interval (cm)	Depth (mbsf)	Sed. temp.* (°C)	Methane	
			HS (ppm)	VAC (ppm)
155-946A-				
1H-2, 0-5	1.50	2	3	
2H-4, 0-5	11.55	2	14,377	
3H-6, 0-5	24.00	3	8,304	231,939
4H-5, 0-5	31.90	3	8,371	476,013
5H-5, 0-5	41.50	3	5,874	25,928
6H-7, 140-145	53.10	4	4,750	
7H-2, 0-5	56.00	4	8,221	
8H-6, 0-5	72.90	4	5,110	
9H-5, 0-5	79.50	5	6,757	
10H-2, 0-5	84.50	5	5,818	
11H-4, 0-5	97.00	5	6,196	
12H-4, 0-5	106.50	6	9,411	
13X-6, 0-5	116.20	7	13,129	164,714
14X-6, 0-5	128.03	7	5,021	
15X-2, 0-5	131.98	7		520,455
16X-4, 0-5	144.50	8	6,469	
17X-4, 0-5	154.10	8	8,605	
18X-1, 0-5	159.20	9	7,024	
21X-2, 0-5	189.70	10	4,365	
23X-2, 0-5	209.00	11	7,537	
24X-3, 0-5	220.10	11	6,677	
29X-5, 0-5	271.40	13	6,097	

Notes: HS = headdress; VAC = vacutainer. Geothermal gradient = 43°C/km. Bottom-water temperature = 2°C. *See "In-situ Temperature Measurements" section, this chapter.

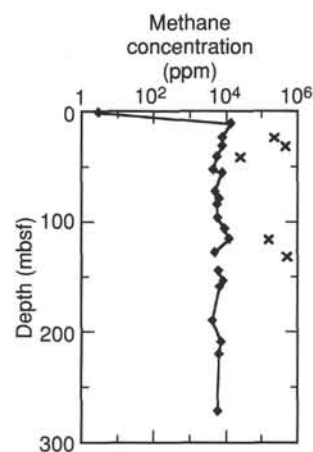


Figure 19. Methane concentrations at Site 946. Headspace (diamond) and vacutainer (x) samples are plotted.

38.3 mM near the bottom of the hole (271.30 mbsf). Calcium concentrations decrease from 10.1 mM at 1.45 mbsf to 5.4 mM at 11.50 mbsf. Below 11.50 mbsf, the concentrations remain between 5.1 and 6.1 mM downhole (Fig. 21F). Pore-water sulfate concentrations decrease from 20.7 mM at 1.45 mbsf to essentially zero by 11.45 mbsf. The concentrations remain near zero downhole, except in the two lowermost samples (sampled by XCB), which have concentrations up to 2.3 mM (Fig. 21G). Ammonium concentrations initially increase with depth from 0.5 mM at 1.45 mbsf to 7.2 mM by 31.85 mbsf (Fig. 21H). Concentrations then gradually decrease to 2.8 mM by 131.88 mbsf, and increase again to a concentration of 6.9 mM in the deepest sample (271.30 mbsf).

Pore-water phosphate concentrations are highest, 56.3 μ M, at 1.45 mbsf. Thereafter, the concentrations vary between 6.3 and 43.2 μ M with no overall downhole trend (Fig. 21I). Dissolved silica concentrations are fairly uniform throughout the hole, varying from 316 to 453 μ M (Fig. 21J). Dissolved potassium concentrations decrease from 11.8 mM at 1.45 mbsf to 8.1 mM by 11.50 mbsf and remain between 9.1 and 7.0 mM for the remainder of the hole (Fig. 21K). The sodium profile shows an initial sharp decrease in concentrations from 469 mM at 1.45 mbsf to 451 mM at 23.95 mbsf. Below 23.95 mbsf, the concentration gradually increases to 477 mM by 131.88 mbsf, and then decreases to 459 mM in the deepest sample (271.30 mbsf) (Fig. 21L). Dissolved iron concentrations increase from 27.4 at 1.45 mbsf to a maximum of 142.2 μ M at 31.85 mbsf (Fig. 21M). The concentrations then decrease to 15.8 μ M by 82.45 mbsf, and remain low, between 6.4 and 18.8 μ M, for the remainder of the hole. Manganese concentrations decrease from 26.4 at 1.45 mbsf to 3.4 μ M at 11.50 mbsf (Fig. 21N). Concentrations remain between 2.4 and 10.4 μ M for the rest of the hole.

PHYSICAL PROPERTIES

Index Properties

Index properties were determined for intact, predominantly clayey sediment beds in Hole 946A (Table 9). Measurements in sand were limited to grain density determinations. Single samples from Units I and II have water contents of 48% and 52%, respectively. Within Unit III, water content decreases with depth from 48% to about 28% (Fig. 22). Between 14 mbsf and 23 mbsf, water content remains relatively constant. Within Units IV through VII, there is a general decrease downhole from 32% to 24% but with a wide scatter. Carbonate-rich sediment tends to have higher water content (e.g., samples from Sections 946A-16X-1, -2, and -5; -17X-2; and -24X-1, -2, and -3).

Table 7. Elemental and organic carbon compositions of sediments from Site 946.

Core, section, interval (cm)	Depth (mbsf)	IC (%)	CaCO ₃ * (%)	TC (%)	TOC (%)	TN (%)	TS (%)	[C/N]a	Lith. unit
155-946A-1H-1, 68-69	0.68	0.06	0.5	0.69	0.63	0.09	0.14	8	II
2H-3, 50-51	10.55	0.20	1.7	1.05	0.85	0.11	0.05	9	
3H-4, 39-40	21.39	0.30	2.5	1.25	0.95	0.12	0.04	10	
4H-4, 107-108	31.57	0.27	2.2	1.23	0.96	0.14	0.03	8	
5H-5, 63-64	42.13	0.08	0.7	4.19	4.11	0.15	0.11	32	
5H-6, 95-96	43.95	0.34	2.8	1.07	0.73	0.09	0.05	9	
6H-6, 51-53	53.01	0.23	1.9	1.55	1.32	0.12	0.10	13	III
7H-1, 90-91	55.40	1.54	12.8	2.45	0.91	0.12	0.04	9	
8H-6, 117-118	72.67	0.46	3.8	1.32	0.86	0.12	0.02	9	
9H-2, 75-77	75.75	0.23	1.9	0.91	0.68	0.11	0.09	7	
10H-2, 97-98	85.47	0.38	3.2	1.57	1.19	0.11	0.06	13	
12H-3, 74-75	105.74	0.27	2.2	1.10	0.83	0.11	0.02	9	
12H-3, 129-130	106.29	0.28	2.3	1.04	0.76	0.09	0.06	10	
15H-1, 44-45	130.94	0.71	5.9	1.07	0.36	0.10	0.14	4	
15H-3, 44-45	133.31	2.20	18.3	2.58	0.38	0.10	0.04	4	
15H-3, 116-117	134.03	0.12	1.0	0.66	0.54	0.09	0.03	7	
16X-3, 3-4	143.03	2.20	18.3	2.51	0.31	0.09	0.00	4	
16X-3, 5-10	143.05	2.57	21.4	2.91	0.34	0.08	0.00	5	
16X-4, 125-130	145.75	3.87	32.2	4.27	0.40	0.08	0.04	6	IV
16X-4, 77-78	145.27	0.28	2.3	0.56	0.28	0.10	0.02	3	
16X-5, 0-20	146.00	0.80	6.7	1.35	0.55	0.09	0.00	7	
16X-6, 80-81	148.30	0.78	6.5	1.33	0.55	0.11	0.00	6	
16X-6, 105-115	148.55	4.26	35.5	4.65	0.39	0.11	0.00	4	
17X-3, 44-45	153.04	1.48	12.3	2.05	0.57	0.09	0.05	7	
17X-CC, 65-66	159.22	0.43	3.6	1.31	0.88	0.11	0.07	10	V

Note: * = calculated assuming all IC is calcite.

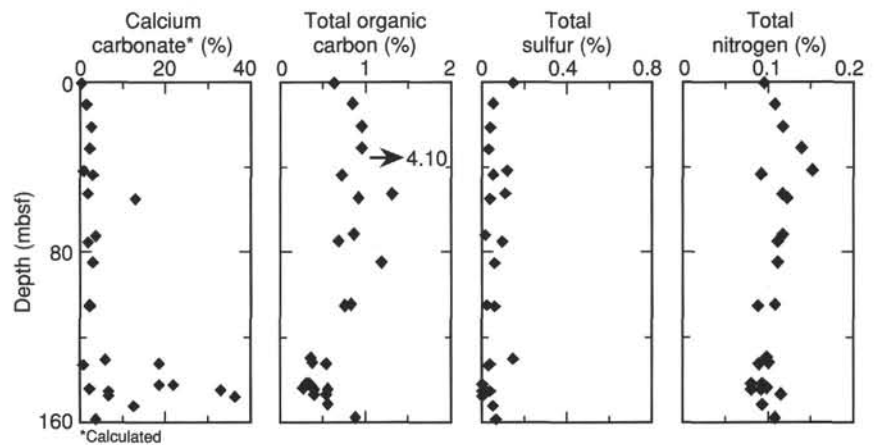


Figure 20. Concentration profiles of carbonate, total organic carbon, total sulfur, and total nitrogen at Site 946.

Grain density variation is primarily in the range between 2.68 g/cm³ and 2.85 g/cm³ (Fig. 22). Overall, grain density increases slightly downhole with a decrease in variability. Grain density averages 2.75 g/cm³ for clayey samples and 2.71 g/cm³ for sand and silt (Table 9).

Porosity and wet-bulk density follow trends similar to those shown by water content (Fig. 22). Porosity is highest (74%) in Unit II, decreases downhole from 71% to 53% in Unit III, and is approximately 46% at the base of Hole 946A. The corresponding wet-bulk density values are 1.50 g/cm³ in Unit II, 1.56 to 1.95 g/cm³ in Unit III, and 2.00 g/cm³ at the base of the hole. The difference between the discrete-sample wet-bulk densities and the GRAPE densities increases over the upper 10 m from 0.2 g/cm³ to 0.4 g/cm³ (Fig. 22). Below this depth, the GRAPE densities remain about 0.4 g/cm³ less than the discrete-sample values. Except for the increased GRAPE densities for the sand of Core 946A-6H, between 45 and 52 mbsf, the GRAPE and discrete-sample data display similar trends.

Compressional-wave Velocity

Pervasive microfractures in sediment affected by gas expansion restricted PWL measurements to the interval from the seafloor to 5.6 mbsf and the interval between 110.17 and 110.37 mbsf. Within the

upper interval, velocities vary considerably, with measurements of 1450 m/s to 1510 m/s for clayey sediment and higher velocities (up to 1650 m/s) that correspond with individual sand and silt layers/laminae (Fig. 23). Between 110.17 mbsf and 110.37 mbsf a peak velocity of 1679 m/s was measured. Although this velocity agrees well with borehole velocity measurements, it is likely that the sand of this interval has been disturbed during coring.

Longitudinal and transverse velocity were measured for clayey sediment from seafloor to 3.80 mbsf using the DSV. A single longitudinal velocity measurement in Unit I gave 1535 m/s, whereas three measurements in Units II and III range from 1503 m/s to 1509 m/s. Single transverse velocity measurements of Units I, II, and III were 1560 m/s, 1524 m/s, and 1539 m/s, respectively.

Shear Strength

Measurements of undrained shear strength were made using the motorized shear vane on most cores (Table 10). Below 74 mbsf, compressive strengths were determined using a pocket penetrometer.

Shear strengths measured in Units I and II are 7.4 kPa and 3.6 kPa, respectively (Fig. 24). Within Unit III, shear strength increases downhole from 6.3 kPa to about 50 kPa at 90 mbsf. Below 90 mbsf,

Table 8. Interstitial water chemistry, Site 946.

Core, section, interval (cm)	Depth (mbsf)	Salinity	pH	Alkalinity (mM)	Cl ⁻ (mM)	Mg ²⁺ (mM)	Ca ²⁺ (mM)	K ⁺ (mM)	HPO ₄ ²⁻ (μM)	SO ₄ ²⁻ (mM)	NH ₄ ⁺ (mM)	H ₄ SiO ₄ (μM)	Na ⁺ (mM)	Fe ²⁺ (μM)	Mn ²⁺ (μM)
155-946A-															
1H-1, 145-150	1.45	34.0	7.61	9.49	552	51.0	10.1	11.8	56.3	20.7	0.5	333	469	27.4	26.4
2H-3, 145-150	11.50	32.0	7.61	13.51	553	42.5	5.4	8.1	37.3	0.5	5.2	410	459	79.4	3.4
3H-5, 145-150	23.95	32.0	7.52	9.58	555	44.5	5.7	8.2	7.3	0.9	7.0	335	451	100.8	3.2
4H-4, 135-140	31.85	32.0	7.49	10.37	557	45.6	5.4	7.4	25.6	0.3	7.2	391	451	142.2	4.0
5H-4, 145-150	41.45	32.0	7.59	10.40	559	44.2	5.2	7.1	7.3	0.8	6.5	439	458	74.2	4.2
8H-6, 145-150	72.95	33.0	7.63	11.97	562	44.9	5.5	7.8	12.1	0.4	4.0	342	462	63.6	4.8
9H-4, 145-150	79.45	32.5	7.57	11.08	564	45.6	6.1	8.1	34.1	0.2	4.9	333	460	87.8	3.8
9H-6, 145-150	82.45	32.5	7.44	10.89	565	46.2	5.8	7.6	6.3	0.2	5.0	316	459	15.8	3.6
12H-3, 140-150	106.40	32.0	7.70	12.29	564	44.9	5.8	8.0	14.6	0.3	4.3	318	463	18.4	2.8
15H-1, 117-127	131.88	32.0	7.92	26.28	549	43.0	5.5	9.1	43.2	0.2	2.8	319	467	9.3	10.4
21X-2, 140-150	191.10	32.0	7.57	13.78	545	36.4	5.1	8.3	18.3	0.4	5.7	402	463	9.1	2.4
24X-2, 140-150	220.00	32.0	7.61	11.49	545	37.8	5.7	7.5	12.9	1.6	4.8	453	461	6.4	7.6
29X-4, 140-150	271.30	32.0	7.62	10.33	546	38.3	6.0	7.0	17.1	2.3	6.9	374	459	18.8	3.4

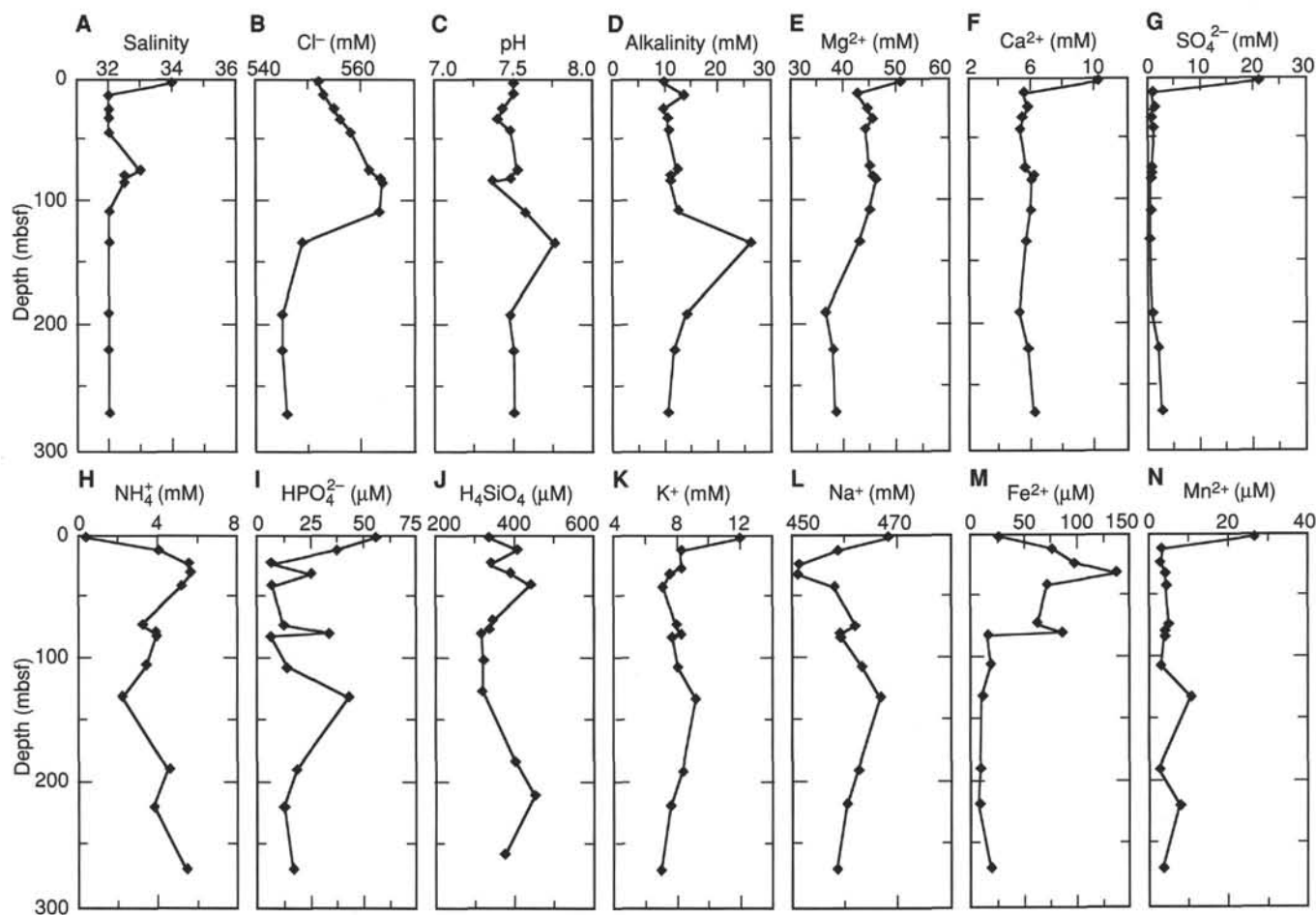


Figure 21. Downhole variation in pore-water chemistry. A. Salinity. B. Chloride. C. pH. D. Alkalinity. E. Magnesium. F. Calcium. G. Sulfate. H. Ammonium. I. Phosphate. J. Silica. K. Potassium. L. Sodium. M. Iron. N. Manganese.

there is no overall increase in shear strength within Unit III. Unit IV has significantly higher shear strength with a maxima of 146 kPa at 132 mbsf. These higher values may result from drainage through the overlying sand, partial cementation of the carbonates, or the low sedimentation rate of the carbonate-rich deposits. Shear strengths decrease overall downhole to 160 mbsf. The few measurements below 160 mbsf suggest strength increases within individual cores, compa-

table to coring-induced reductions in shear strength noted in XCB cores at other Leg 155 sites.

Resistivity

Longitudinal and transverse resistivity were determined for Hole 946A (Table 11). Longitudinal resistivity is 0.37 Ωm at 0.26 mbsf

Table 9. Index properties at Site 946.

Core, section, interval (cm)	Depth (mbsf)	Water content (%)	Wet-bulk density (g/cm ³)	Grain density (g/cm ³)	Dry-bulk density (g/cm ³)	Porosity (%)	Void ratio
155-946A-							
1H-1, 25-27	0.25	48.4	1.59	2.58	0.77	70.2	2.36
1H-1, 101-103	1.01	52.1	1.50	2.70	0.70	74.1	2.87
1H-2, 121-123	2.71	48.1	1.56	2.72	0.79	71.1	2.46
1H-3, 79-81	3.79	46.4	1.57	2.66	0.82	69.3	2.25
1H-4, 136-138	5.86	42.4	1.65	2.77	0.93	66.5	1.99
1H-5, 76-78	6.76	41.4	1.69	2.81	0.96	66.0	1.94
2H-1, 118-120	8.18	38.7	1.71	2.76	1.02	62.9	1.70
2H-2, 118-120	9.73	37.4	1.73	2.71	1.05	61.3	1.58
2H-3, 118-120	11.23	39.4	1.68	2.69	0.99	63.1	1.71
2H-4, 123-125	12.78	38.8	1.72	2.76	1.02	63.1	1.71
2H-5, 96-98	14.01	37.7	1.72	2.69	1.04	61.4	1.59
2H-6, 58-60	15.13	37.6	1.72	2.67	1.04	61.1	1.57
3H-1, 115-117	17.65	37.3	1.73	2.72	1.05	61.2	1.58
3H-2, 62-64	18.62	37.4	1.72	2.68	1.05	61.1	1.57
3H-3, 104-106	20.54	37.1	1.73	2.77	1.07	61.5	1.60
3H-4, 120-122	22.20	37.2	1.72	2.73	1.06	61.2	1.58
3H-5, 95-97	23.45	36.8	1.76	2.75	1.07	61.0	1.57
3H-6, 38-40	24.38	37.4	1.74	2.77	1.06	61.7	1.61
3H-7, 60-62	26.10	35.0	1.78	2.72	1.12	58.9	1.43
4H-1, 49-51	26.49	34.5	1.77	2.74	1.14	58.4	1.41
4H-2, 128-130	28.78	35.4	1.78	2.78	1.12	59.7	1.48
4H-3, 83-85	29.83			2.67			
4H-4, 91-93	31.41	35.4	1.76	2.70	1.10	59.1	1.44
4H-5, 67-69	32.57	33.5	1.79	2.69	1.16	57.0	1.33
4H-6, 4-6	33.44	36.1	1.75	2.66	1.08	59.4	1.46
4H-7, 17-19	35.07	34.0	1.80	2.74	1.15	57.9	1.38
5H-1, 41-43	35.91	31.9	1.82	2.69	1.21	55.2	1.23
5H-2, 38-40	37.38	32.4	1.80	2.70	1.19	55.9	1.27
5H-3, 42-44	38.92	32.7	1.81	2.70	1.18	56.2	1.28
5H-4, 122-124	41.22	33.4	1.80	2.71	1.16	57.1	1.33
5H-5, 53-55	42.03			2.58			
5H-6, 103-105	44.03	31.7	1.84	2.76	1.23	55.5	1.25
6H-2, 99-101	47.49			2.67			
7H-1, 100-102	55.50	34.4	1.76	2.92	1.17	59.9	1.49
7H-2, 80-82	56.80			2.76			
7H-3, 117-119	58.67	31.2	1.76	2.90	1.27	56.2	1.28
7H-4, 64-66	59.64	32.8	1.81	2.85	1.21	57.6	1.36
7H-5, 14-16	60.64	30.5	1.86	2.79	1.27	54.4	1.19
7H-5, 142-144	61.92			2.70			
8H-1, 90-92	64.90	32.2	1.82	2.72	1.20	55.7	1.26
8H-2, 90-92	66.40			2.73			
8H-3, 92-94	67.92	30.9	1.84	2.72	1.25	54.3	1.19
8H-4, 88-90	69.38	33.3	1.80	2.73	1.17	57.1	1.33
8H-5, 43-45	70.43	31.8	1.83	2.78	1.23	55.9	1.27
8H-6, 128-130	72.78	30.1	1.85	2.76	1.28	53.7	1.16
8H-7, 25-27	73.25	28.1	1.92	2.77	1.35	51.4	1.06
9H-1, 92-94	74.42	30.4	1.84	2.69	1.25	53.5	1.15
9H-2, 92-94	75.92	30.5	1.84	2.72	1.26	53.8	1.16
9H-3, 118-120	77.68	28.6	1.90	2.77	1.33	52.0	1.08
9H-4, 83-85	78.83	29.4	1.89	2.73	1.30	52.6	1.11
9H-5, 70-72	80.20			2.72			
9H-6, 70-72	81.70			2.67			
9H-6, 123-125	82.23	34.0	1.80	2.82	1.16	58.7	1.42
10H-1, 122-124	84.22	30.3	1.86	2.70	1.26	53.4	1.15
10H-2, 78-80	85.28			2.73			
11H-1, 121-123	93.71	28.5	1.90	2.72	1.32	51.4	1.06
11H-2, 37-39	94.37	29.2	1.89	2.78	1.31	52.8	1.12
11H-3, 63-65	96.13	35.5	1.78	2.86	1.13	60.5	1.53
11H-4, 108-110	98.08	28.7	1.91	2.78	1.33	52.2	1.09
11H-5, 58-60	99.08			2.75			
11H-6, 116-118	101.16			2.71			
11H-7, 33-35	101.83	30.1	1.86	2.74	1.27	53.5	1.15
12H-1, 11-13	102.11	33.6	1.80	2.77	1.17	57.9	1.37
12H-1, 88-90	102.88			2.69			
12H-2, 22-24	103.72	31.6	1.87	2.81	1.24	55.9	1.27
12H-3, 88-90	105.88	28.0	1.90	2.73	1.34	50.9	1.04
12H-4, 12-14	106.62	27.0	1.99	2.84	1.40	50.6	1.02
12H-5, 91-93	107.73			2.72			
12H-6, 91-93	109.23			2.74			
13H-1, 64-66	112.14			2.70			
13H-2, 67-69	113.67			2.77			
13H-2, 135-137	114.35	27.7	1.96	2.78	1.36	51.0	1.04
13H-3, 40-42	114.90	28.4	1.93	2.79	1.34	51.9	1.08
13H-3, 135-137	115.85			2.73			
13H-4, 88-90	116.88	28.4	1.95	2.86	1.36	52.6	1.11
14H-1, 21-23	121.21	33.3	1.81	2.78	1.18	57.5	1.35
14H-2, 60-62	122.63			2.68			
14H-3, 60-62	124.13			2.69			
14H-4, 60-62	125.63			2.69			
14H-5, 60-62	127.13			2.71			
14H-6, 128-130	129.31	32.3	1.84	2.73	1.20	55.9	1.27
14H-7, 53-55	130.06	30.7	1.91	2.83	1.27	55.0	1.22
15H-1, 105-107	131.55	28.1	1.94	2.66	1.32	50.4	1.02
15H-4, 125-127	135.62	28.1	1.92	2.73	1.34	51.0	1.04
15H-5, 127-129	137.14	29.3	1.96	2.84	1.32	53.5	1.15
16X-1, 81-83	140.81	33.9	1.80	2.74	1.16	57.8	1.37
16X-2, 82-84	142.32	33.2	1.81	2.69	1.17	56.7	1.31

Table 9 (continued).

Core, section, interval (cm)	Depth (mbsf)	Water content (%)	Wet-bulk density (g/cm ³)	Grain density (g/cm ³)	Dry-bulk density (g/cm ³)	Porosity (%)	Void ratio
16X-3, 60-62	143.60	28.9	1.91	2.74	1.31	52.0	1.08
16X-4, 61-63	145.11	28.6	1.97	2.79	1.33	52.2	1.09
16X-5, 77-79	146.77	35.5	1.80	2.79	1.12	60.0	1.50
16X-6, 53-55	148.03	29.8	1.87	2.73	1.28	53.0	1.13
17X-1, 73-75	150.33	32.4	1.83	2.73	1.20	56.1	1.28
17X-2, 54-56	151.64	31.8	1.85	2.68	1.21	54.9	1.22
17X-4, 32-34	154.42	33.2	1.83	2.82	1.19	57.8	1.37
17X-5, 86-88	156.46	27.0	1.98	2.82	1.40	50.5	1.02
17X-6, 113-115	158.23	27.9	1.93	2.70	1.34	50.6	1.02
18X-1, 97-99	160.17	27.6	1.91	2.73	1.35	50.4	1.02
21X-1, 112-114	189.32	28.1	1.91	2.79	1.35	51.6	1.07
21X-3, 134-136	192.54	24.9	1.97	2.77	1.46	47.3	0.90
23X-1, 64-66	208.14	27.5	1.92	2.78	1.37	50.8	1.03
23X-2, 38-40	209.38	26.6	1.91	2.72	1.39	49.0	0.96
23X-3, 54-56	211.04	27.5	1.94	2.79	1.37	50.8	1.03
24X-1, 52-54	217.62	29.6	1.88	2.76	1.30	53.1	1.13
24X-2, 101-103	219.61	27.3	1.90	2.73	1.36	50.0	1.00
24X-3, 23-25	220.33	28.4	1.91	2.78	1.34	51.8	1.08
29X-1, 111-113	266.51	26.9	1.96	2.76	1.38	49.8	0.99
29X-2, 111-113	268.01	24.5	1.99	2.75	1.47	46.6	0.87
29X-3, 111-113	269.51	24.8	1.99	2.77	1.46	47.2	0.89
29X-4, 57-59	270.47	24.0	2.01	2.75	1.49	45.9	0.85
29X-5, 32-34	271.72	24.2	2.00	2.74	1.48	46.1	0.85
29X-6, 32-34	273.22	24.5	2.00	2.78	1.48	46.8	0.88

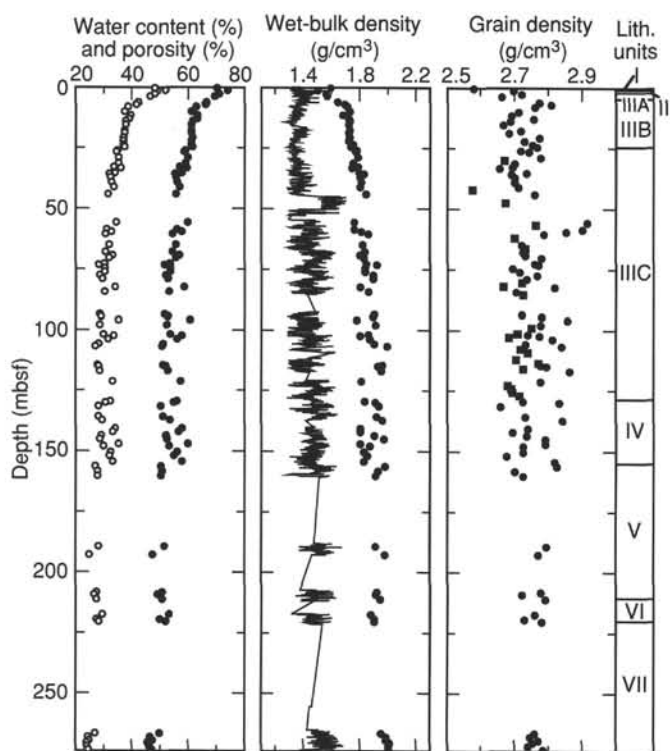


Figure 22. Water content (open circles) and porosity (solid circles), wet-bulk density as determined for discrete samples (circles) and by the GRAPE (line), and grain density in Hole 946A. Silt and sand sampled only for grain density are represented by squares.

(Unit I) and $0.27 \Omega\text{m}$ at 1.02 mbsf (Unit II). Within Unit III resistivity increases from $0.22 \Omega\text{m}$ to $0.63 \Omega\text{m}$ at 121 mbsf (Fig. 25). Resistivity measurements greater than the general trend occur between 5.8 mbsf and 8.2 mbsf. Below 128 mbsf (Units IV through VII), resistivity remains generally constant ($0.46\text{--}0.56 \Omega\text{m}$)

Comparison of longitudinal and transverse resistivities indicates that sediment types in Hole 946A are slightly anisotropic with an average anisotropy of -2.3% (Fig. 25). Between 2 and 18 mbsf, the change in anisotropy to increasing negativity coincides with increasing frequency of sand and silt laminae.

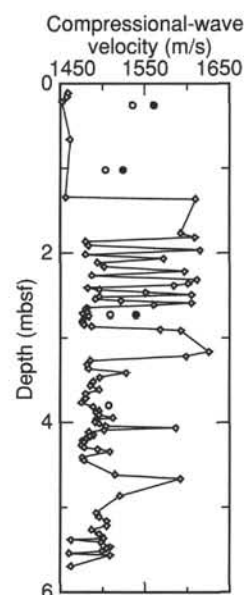


Figure 23. Uncorrected compressional-wave velocity measurements, from PWL (line with diamonds at measurement levels) and DSV: longitudinal (open circles) and transverse (solid circles).

DOWNHOLE LOGGING

Logging Operations and Quality of Logs

After drilling was completed, we raised the drill pipe to 98 mbsf, then returned to the total drilled depth (TD) of 275 mbsf to ream the borehole. Seven meters of fill was encountered in the bottom of the hole. Sepiolite mud mixed with seawater (1.055 g/cm^3) was pumped into the borehole and circulated to remove debris. A second sepiolite-seawater mix was added to the borehole to help maintain borehole stability during logging. Both the Quad-combination and FMS tool strings reached TD, and useful logs were obtained from 274 to 78 mbsf (Table 12).

The borehole diameter was obtained only from the FMS calipers, because the density tool (HLDT) caliper malfunctioned at about 250 mbsf. Although the HLDT caliper measured inaccurate values, den-

Table 10. Undrained shear strength at Site 946.

Core, section, interval (cm)	Depth (mbsf)	Peak undrained shear strength (kPa)	Residual undrained shear strength (kPa)	Unconfined compressive strength* (kPa)
155-946A-				
1H-1, 26	0.26	7.4	4.8	
1H-1, 102	1.02	3.6	2.7	
1H-2, 122	2.72	6.3	4.6	
1H-3, 80	3.80	7.2	4.8	
1H-4, 137	5.87	9.0	5.9	
1H-5, 77	6.77	8.0	5.6	
2H-1, 119	8.19	8.7	6.6	
2H-2, 119	9.74	10.1	6.9	
2H-3, 119	11.24	9.6	7.2	
2H-4, 124	12.79	12.3	8.6	
2H-5, 97	14.02	11.3	7.6	
2H-6, 59	15.14	11.0	7.6	
3H-1, 116	17.66	17.2	11.1	
3H-2, 63	18.63	23.2	13.1	
3H-3, 105	20.55	13.3	10.1	
3H-4, 121	22.21	15.3	10.6	
3H-5, 96	23.46	13.3	9.7	
3H-6, 39	24.39	13.6	9.2	
3H-7, 61	26.11	13.0	9.3	
4H-1, 50	26.50	19.2	12.8	
4H-2, 128	28.78	16.4	11.3	
4H-4, 91	31.41	23.5	15.2	
4H-5, 67	32.57	24.6	13.8	
4H-6, 5	33.45	26.0	14.2	
4H-7, 17	35.07	20.7	13.5	
5H-1, 41	35.91	17.3	11.5	
5H-2, 39	37.39	26.6	16.0	
5H-3, 43	38.93	27.7	16.5	
5H-6, 104	44.04	21.2	13.3	
7H-1, 100	55.50	56.0	26.2	
7H-3, 117	58.67	61.4	27.8	
7H-4, 66	59.66	48.4	25.5	
8H-1, 91	64.91	32.4	18.9	
8H-3, 93	67.93	37.5	21.3	
8H-4, 88	69.38	47.3	17.8	
8H-5, 43	70.43	39.6	18.9	
8H-6, 128	72.78	38.1	15.7	
8H-7, 26	73.26	45.8	23.9	
9H-1, 92	74.42	25.2	14.8	54.0
9H-2, 92	75.92	67.9	30.3	166.8
9H-3, 120	77.70	49.9	30.3	98.1
9H-4, 84	78.84	46.8	27.4	103.0
9H-6, 125	82.25	36.0	15.9	73.6
10H-1, 122	84.22	45.3	19.0	112.8

Core, section, interval (cm)	Depth (mbsf)	Peak undrained shear strength (kPa)	Residual undrained shear strength (kPa)	Unconfined compressive strength* (kPa)
11H-1, 122	93.72			63.8
11H-4, 110	98.10	48.3	18.9	63.8
11H-7, 34	101.84	47.8	16.8	112.8
12H-1, 12	102.12	18.0	10.8	29.4
12H-2, 23	103.73	19.0	11.0	29.4
12H-3, 89	105.89	40.1	19.5	88.3
12H-6, 13	108.45			54.0
13H-2, 136	114.36	46.3	17.8	98.1
13H-3, 41	114.91	45.8	24.4	112.8
13H-4, 89	117.00	51.4	21.6	137.3
14H-1, 22	121.00	35.0	22.2	98.1
14H-6, 129	129.32	105.2	41.8	206.0
14H-7, 54	130.07	112.3	59.0	210.9
15H-1, 106	131.56	145.9	64.6	245.3
15H-4, 126	135.63	133.5	66.0	255.1
15H-5, 128	137.15	95.5	46.8	215.8
16X-1, 82	140.82	93.1	28.0	152.1
16X-2, 83	142.33	84.9	30.0	122.6
16X-3, 61	143.61	81.3	30.0	127.5
16X-4, 62	145.12	81.3	31.0	161.9
16X-5, 78	146.78	96.4	32.0	152.1
16X-6, 54	148.04	94.6	26.0	152.1
17X-1, 74	150.34	43.3	18.0	93.2
17X-2, 55	151.65	47.7	24.0	98.1
17X-4, 33	154.43	44.2	24.3	98.1
17X-5, 87	156.47	71.6	39.0	157.0
17X-6, 114	158.24	81.3	39.3	166.8
18X-1, 98	160.18	59.2	29.4	107.9
21X-1, 112	189.32	31.8	13.5	68.7
21X-3, 134	192.54	48.6	30.1	117.7
23X-1, 65	208.15	69.8	23.6	98.1
23X-2, 37	209.37	55.7	32.6	132.4
23X-3, 55	211.05			117.7
24X-1, 54	217.64	70.7	26.0	117.7
24X-2, 102	219.62	72.5	20.1	166.8
24X-3, 23	220.33	70.7	36.2	210.9
29X-1, 111	266.51	42.4	22.0	117.7
29X-2, 111	268.01	58.3	30.1	157.0
29X-3, 111	269.51	85.8	35.3	196.2
29X-4, 58	270.48	91.1	46.5	186.4
29X-5, 65	272.05	97.2	37.3	245.3
29X-6, 32	273.22	110.5	60.2	260.0

Note: *Unconfined compressive strength (q_u) can be used to approximate undrained shear strength (S_u) by the relationship $q_u = 2S_u$.

sity data appear to be of good quality and indicate that the HLDT pad sensor was in contact with the borehole wall. Anomalously low densities occur over small washed-out intervals where borehole diameter (from FMS caliper) exceeded 15.5 in. (39 cm) and probably caused intermittent loss of contact of the HLDT pad with the borehole wall.

FMS images were obtained during two passes, and these data are of good quality. Over short intervals, where the borehole diameter was greater than the maximum aperture of the tool calipers (39 cm), poor FMS pad contact resulted in degraded images. During the second pass of the FMS tool, the pads appeared to follow the same track; additional borehole coverage was obtained only within a few intervals.

Comparison of logging data with core lithology indicates that the logging depths are about 3 m shallower than core depths. The gamma-ray log indicated the position of the bottom-hole assembly (BHA) during the downgoing run to be at 99.5 mbsf (4211 mbrf), instead of 97.6 mbsf, indicated by the drill-pipe measurement. During the upgoing run of the FMS tool string, the BHA and seafloor were detected at 4190 and 4111 mbrf, respectively, in good agreement with the drill-pipe measurement. Shore-based processed and depth-shifted logs are shown at the end of this chapter and in the enclosed CD-ROM (back pocket).

Results

Logging data covers sections of low core recovery below 162 mbsf and provides ground-truth of key interpretations in high core recovery intervals above 162 mbsf (Fig. 26). Logging data were ob-

tained for the lower half of lithostratigraphic Subunit IIIC and for Units IV, V, VI, and VII (Fig. 26).

Subunit IIIC is characterized by relatively low gamma-ray counts and neutron porosity, and by three 8- to 10-m-thick intervals having high velocity and density values (85–93, 102–109, and 115–125 mbsf). These intervals correlate well with the sand-rich beds recovered in the cores. Intervals of sand with mud clasts (e.g., between 110 and 115 mbsf) show higher resistivity and gamma-ray responses (Fig. 27A). It appears that the thick sand beds recovered in the cores between 90 and 127 mbsf have not been significantly deformed by APC flow-in.

Below 125 mbsf, an abrupt increase in gamma ray and neutron porosity is accompanied by a sharp decrease in velocity and density. This increase probably corresponds to the contact between Units III and IV, observed at 128 mbsf in the cores. Gamma-ray counts are overall high between 125 and 159 mbsf, but decrease slightly in the middle of the section, probably due to a higher carbonate content (Fig. 27A). Resistivity within Unit IV exhibits minimum values at 139 and 156 mbsf, with intervening high values that are particularly well defined in the shallow resistivity data. We interpret the low resistivity intervals as representing the bioturbated clay that is rich in authigenic iron, whereas the high resistivity values probably correspond to the carbonate-rich clay intervals. If this interpretation is correct, the interval of no recovery between 137.5 and 140 mbsf probably comprises laminated silty clays similar to those in the lower part of Core 946A-15H between 135 and 137.5 mbsf (Fig. 27A).

An abrupt decrease in gamma-ray values below 159 mbsf is accompanied by a sharp increase in velocity and density values and by

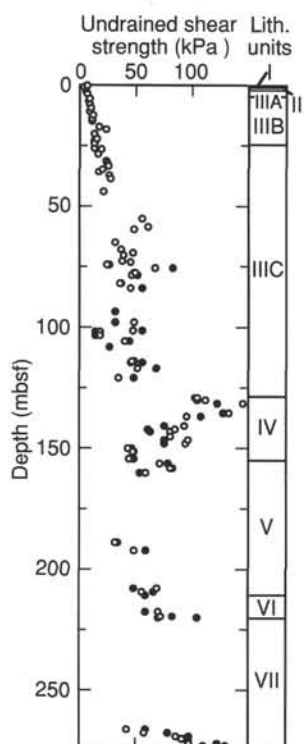


Figure 24. Undrained shear strength (open circles) and assumed undrained shear strength derived from unconfined compressive strength (solid circles) in Hole 946A.

a decrease in neutron-porosity values. This abrupt decrease occurs below the boundary between Units IV and V. Gamma-ray response is generally low within Unit V, except for a few intervals having high counts that appear to correlate to mud-clast conglomerates (Fig. 27A). These mud clasts apparently are responsible for the higher resistivity values. The intervals of low recovery in Unit V generally correspond to low gamma-ray values and low resistivity, which suggests that these are associated with relatively mud-free sand. Well-defined high velocity intervals occur at 161–168, 174–180, 189–199, and 202–208 mbsf (Fig. 26). These intervals indicate logging characteristics that are similar to the sand-rich intervals within Unit III. FMS images suggest that the high-velocity intervals are packets composed of several 0.5- to 1-m-thick beds.

Unit VI is characterized by overall high gamma-ray and low density and velocity values. The unit shows a pronounced decrease in the deep (IDPH) resistivity to low values ($\sim 0.5 \Omega\text{m}$) at 212–214 mbsf, whereas shallow resistivity (SFLU) shows two pronounced high-resistivity peaks within the same interval (Fig. 27B). The carbonate-rich interval at the base of Core 946A-23X appears to correspond to slightly decreased gamma-ray values observed at 208 mbsf in the logs. The changes in resistivity probably are related to the alternation of carbonate-rich clay with authigenic iron-rich intervals.

The contact between Units VI and VII is marked by an abrupt decrease in gamma-ray values at 218 mbsf and by an increase in velocity and density (Figs. 26 and 27B). Two “subunits” can be discerned within Unit VII from the logs. The upper subunit, between 218 and 250 mbsf, is characterized by overall low gamma-ray values, with resistivity, density, and velocity increasing downhole. Between 228 and 232 mbsf, an interval of slightly lower resistivity corresponds to a couplet of velocity peaks. The reason for this is unclear, but it may be related to high borehole ellipticity and partial bridging in the borehole (C1 in Fig. 26). A sharp increase in gamma-ray counts below 250 mbsf defines the top of the lower subunit, between 250 and 262 mbsf. This lower subunit is characterized by two intervals of upward-increasing gamma-ray counts that suggest fining-upward and/or thin-

Table 11. Electrical resistivity at Site 946.

Core, section, interval (cm)	Depth (mbsf)	Longitudinal resistivity (Ωm)	Transverse resistivity (Ωm)
155-946A-			
1H-1, 26	0.26	0.367	0.327
1H-1, 102	1.02	0.270	0.246
1H-2, 122	2.72	0.226	0.245
1H-3, 80	3.80	0.242	0.246
1H-4, 137	5.87	0.285	0.300
1H-5, 77	6.77	0.297	0.300
2H-1, 119	8.19	0.302	0.305
2H-2, 119	9.74	0.263	0.258
2H-3, 119	11.24	0.260	0.258
2H-4, 124	12.79	0.270	0.266
2H-5, 97	14.02	0.264	0.262
2H-6, 59	15.14	0.262	0.251
3H-1, 116	17.66	0.297	0.263
3H-2, 63	18.63	0.283	0.265
3H-3, 105	20.55	0.291	0.282
3H-4, 121	22.21	0.277	0.272
3H-5, 96	23.46	0.266	0.297
3H-6, 39	24.39	0.286	0.281
3H-7, 61	26.11	0.292	0.293
4H-1, 50	26.50	0.340	0.340
4H-2, 128	28.78	0.318	0.310
4H-4, 91	31.41	0.339	0.354
4H-5, 67	32.57	0.350	0.345
4H-6, 5	33.45	0.319	0.322
4H-7, 17	35.07	0.345	0.363
5H-1, 41	35.91	0.363	0.355
5H-2, 38	37.38	0.348	0.335
5H-3, 43	38.93	0.342	0.347
5H-4, 122	41.22	0.331	0.331
5H-6, 104	44.04	0.352	0.333
7H-1, 100	55.50	0.369	0.386
7H-3, 120	58.70	0.362	0.389
7H-4, 66	59.66	0.390	0.397
7H-5, 15	60.65	0.414	0.395
8H-1, 91	64.91	0.418	0.416
8H-3, 93	67.93	0.440	0.440
8H-4, 88	69.38	0.410	0.414
8H-5, 43	70.43	0.408	0.402
8H-6, 128	72.78	0.438	0.436
8H-7, 26	73.26	0.467	0.437
9H-1, 92	74.42	0.410	0.404
9H-2, 92	75.92	0.401	0.399
9H-3, 120	77.70	0.444	0.442
9H-4, 84	78.84	0.440	0.429
9H-6, 125	82.25	0.415	0.392
10H-1, 122	84.22	0.442	0.433
11H-1, 122	93.72	0.467	0.449
11H-2, 39	94.39	0.473	0.434
11H-4, 110	98.10	0.473	0.471
11H-7, 34	101.84	0.469	0.460
12H-1, 12	102.12	0.502	0.517
12H-2, 23	104.00	0.453	0.407
12H-3, 89	106.00	0.429	0.444
12H-6, 13	108.45	0.448	0.412
13H-2, 136	114.36	0.522	0.524
13H-3, 41	114.91	0.520	0.487
13H-4, 89	116.89	0.550	0.565
14H-1, 22	121.22	0.629	0.462
14H-6, 129	129.32	0.475	0.462
14H-7, 54	130.07	0.537	0.516
15H-1, 106	131.56	0.526	0.533
15H-4, 126	135.63	0.548	0.533
15H-5, 128	137.15	0.530	0.492
16X-1, 82	140.82	0.540	0.482
16X-2, 83	142.33	0.536	0.487
16X-3, 61	143.61	0.564	0.505
16X-4, 62	145.12	0.531	0.491
17X-1, 74	150.34	0.522	0.529
17X-2, 55	151.65	0.517	0.526
17X-4, 33	154.43	0.517	0.478
17X-5, 87	156.47	0.538	0.510
17X-6, 114	158.24	0.522	0.505
18X-1, 98	160.18	0.530	0.494
18X-1, 112	189.32	0.467	0.476
18X-3, 134	192.54	0.501	0.501
23X-1, 65	208.15	0.494	0.477
23X-2, 37	209.37	0.537	0.528
23X-3, 55	211.05	0.528	0.520
24X-1, 54	217.64	0.496	0.475
24X-2, 102	219.62	0.459	0.455
24X-3, 23	220.33	0.488	0.467
29X-1, 111	266.51	0.489	0.486
29X-2, 111	268.01	0.516	0.502
29X-3, 111	269.51	0.502	0.500
29X-4, 58	270.48	0.485	0.496
29X-5, 65	272.05	0.500	0.508
29X-6, 32	273.22	0.518	0.502

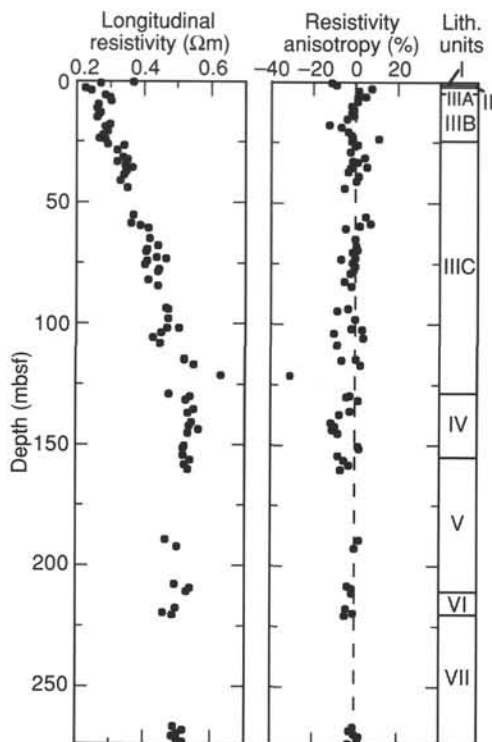


Figure 25. Longitudinal resistivity and resistivity anisotropy in Hole 946A.

ning-upward sequences (Fig. 27B). Below 262 mbsf, we observed high gamma-ray counts and relatively high and uniform resistivity that correlates with the silt-laminated interval recovered at the bottom of the hole. These data indicate that Unit VII is composed mostly of thick-bedded sand, with thin-bedded turbidite sand and silt at its base. FMS images suggest bed thicknesses of up to 3 to 5 m at the top of the unit, which apparently decrease in thickness at its base.

Borehole Temperature

Temperature logs were obtained about 3 hr after circulation of mud and seawater in the borehole (Fig. 28). During the upgoing run, we encountered difficulties when attempting to reenter the drill pipe, and seawater was pumped into the hole. Mud-line temperature of the TLT at 2.2°C is consistent with the value measured by the ADARA. Two abrupt temperature increases occur at 25 and 75 mbsf in pipe. The reason for these sharp increases is unknown. Borehole temperature shows an abrupt increase in temperature gradient between 120 and 150 mbsf. The upper and lower boundaries of this temperature anomaly correspond to abrupt changes in lithology at the upper and bottom contacts of Unit IV and may reflect changes in thermal conductivities in the adjacent formation. Variations in borehole temperature may result from downhole variation in fluid type, because the sepiolite-seawater mix may not have filled the borehole to the mud line. Borehole diameter also increases markedly below about 120

mbsf (Fig. 26) and may have affected borehole fluid convection. The potential effects of fluid convection, stratification, and borehole diameter on the temperature profile should be examined in detail before attempting to interpret the causes of temperature variations.

CORE-SEISMIC INTEGRATION

Sites 945 and 946, located near the middle to lower fan transition, are correlated to a *JOIDES Resolution* seismic profile (Fig. 29; Fig. 2 of “Site 945” chapter, this volume; Site 945 at 1906UTC and Site 946 at 1900UTC on 17 May 1994). Site 945 is located within the main channel of the Amazon system, and Site 946 is located on the eastern levee. Four seismic-facies units were recognized based on 3.5-kHz (Fig. 3 of “Site 945” chapter, this volume) and water-gun reflection profiles. Preliminary correlation between the seismic-facies units and the lithologic units at Site 946 (Fig. 30) was based on the velocity-depth equation determined at Site 931.

Seismic-facies Unit 1, between 0 and 25 ms on the 3.5-kHz profile, is characterized by moderate-amplitude, continuous reflections that diverge toward the channel. This seismic-facies unit correlates to lithologic Units I and II, and Subunit IIIA and the upper part of IIIB (Fig. 30). The strong reflection at the base of seismic-facies Unit 1 appears to correlate with the top of a bioturbated interval at 18 mbsf.

Seismic-facies Unit 2 (25 to 165 ms) is characterized by continuous, subparallel high-amplitude reflections and correlates with the lower parts of lithologic Subunit IIIB and Subunit IIIC, which consist of mud with silt laminae, thin- and thick-bedded turbidites, and thick coarse-sand beds. The prominent reflection at the base of seismic-facies Unit 2 correlates with the contact between lithologic Subunit IIIC and Unit IV at 128 mbsf.

Seismic-facies Unit 3 (165 and 267 ms) is similar to seismic-facies Unit 2 in amplitude but has continuous parallel reflections that diverge slightly to the west. On the *Conrad* water-gun profiles, this interval is less reflective than the overlying and underlying seismic-facies units, and correlates up-fan with either the Lower or Middle Levee Complex. This seismic-facies unit correlates with lithologic Units IV and V, which consist of bioturbated carbonate-rich clays and silty clay, and thin to thick silt beds with poorly sorted fine sand, respectively. The prominent reflector at the base of seismic-facies Unit 3 at 267 ms correlates to the contact between lithologic Units IV and V.

Seismic-facies Unit 4 (267 and 370 ms) is characterized by moderate- to high-amplitude, discontinuous, irregular reflections. These reflections correlate to lithologic Units VI and VII, which are bioturbated calcareous clays and thin-bedded turbidites, respectively.

IN-SITU TEMPERATURE MEASUREMENTS

Temperature gradients and heat flow were determined using one downhole measurement and the bottom-water (mud-line) temperature. An ADARA measurement was attempted during Core 946A-5H, but a reliable equilibrium temperature could not be extrapolated due to tool-induced frictional heating. A second ADARA measurement was made during Core 946A-7H (64 mbsf) using instrument

Table 12. Intervals logged and tools employed in Hole 946A.

String	Run	Open hole		In pipe		Tools
		(mbsf)	(mbrf)	(mbsf)	(mbrf)	
Quad	Down	94.5–274.5	4206–4385			NGT/LSS/CNT-G/HLDT/DITE/TLT
	Up 1	274.5–168.5	4385–4280			
	Up 2	274.5–78.5	4385–4190			
FMS	Up 1	273.5–105.5	4383–4217	78.5–0	4190–4111.5	NGT/GPIT/FMS
	Up 2	273.5–89.5	4383–4201			

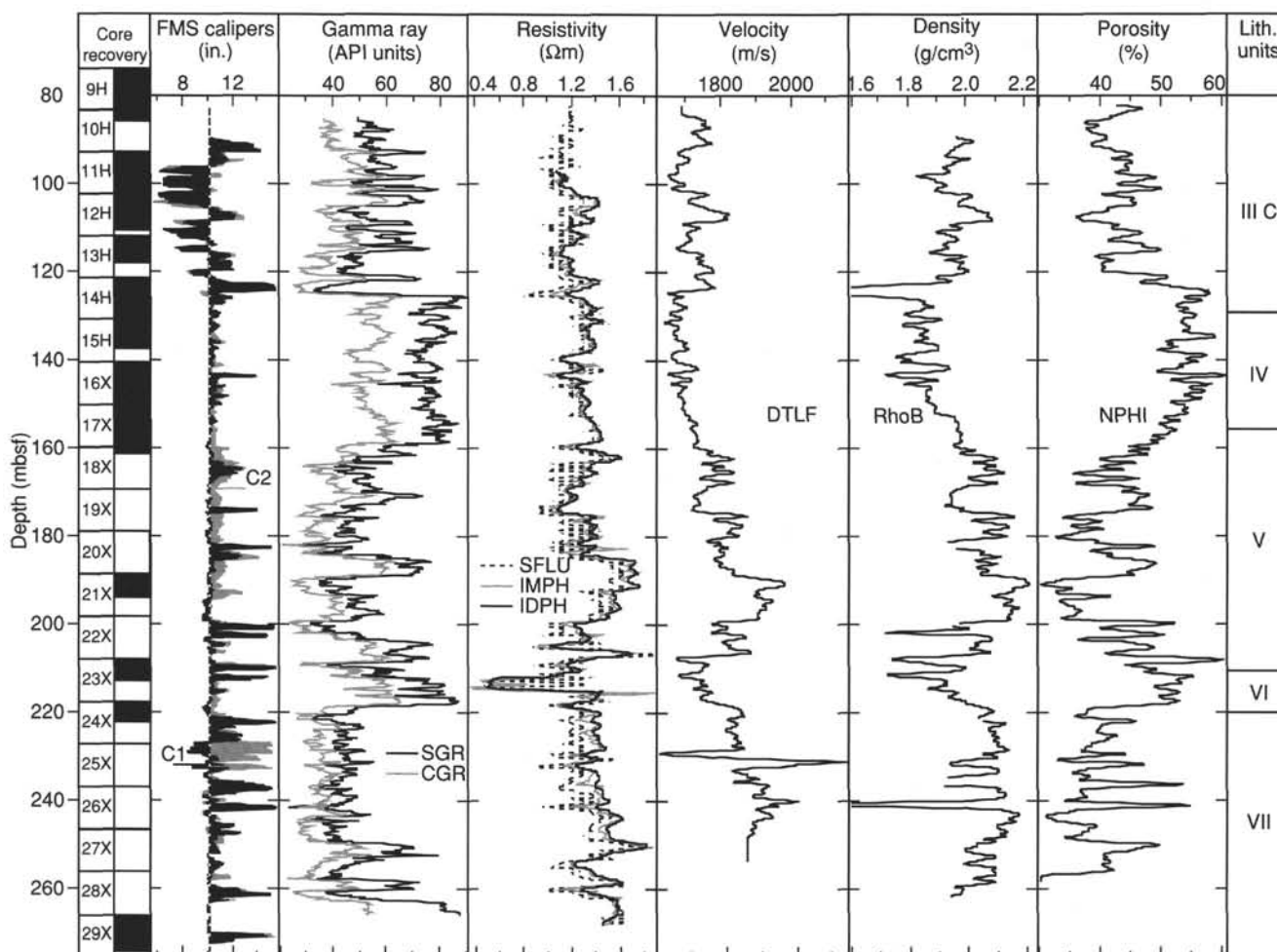


Figure 26. Summary of logging data from the Quad-combination tool string for Hole 946A. Left to right: core recovery diagram; borehole diameter (C1 and C2 are orthogonal caliper measurements from FMS tool string); spectral (SGR) and computed (CGR = Th + K) gamma ray; shallow (SFLU), medium (IMPH), and deep (IDPH) resistivity; long-spacing sonic velocity (DTLF); bulk density (RhoB); and neutron-porosity (NPHI).

number 12. The mud-line temperature of 2.24°C measured from this instrument was used as the reference bottom-seawater temperature at Site 946. A successful measurement resulted in an extrapolated equilibrium temperature of 4.99°C.

The equilibrium temperature, extrapolated from a synthetic curve constructed to fit transient temperature data, is plotted as a function of depth (mbsf) in Figure 31. Using the ADARA mud-line temperature and the sub-bottom temperature from the ADARA measurement downhole, the geothermal temperature gradient can be approximated by a linear mean of 42.9°C/km. We calculated heat flow by adopting the constant geothermal temperature gradient of 42.9°C/km and a linear increase in thermal conductivity, K , of 1.05 ± 0.15 W/(m·K), which is an average of regression estimates at 80 mbsf. This results in a calculated heat flow of 45.07 mW/m².

SYNTHESIS AND SIGNIFICANCE

Stratigraphic Synthesis

Holocene to Latest Pleistocene Bioturbated Sediment (Units I and II)

Unit I (0–0.45 mbsf) is a bioturbated, foraminifer-nannofossil clay, similar to Unit I at previous Leg 155 sites. Unit II (0.45–1.18 mbsf) consists of clay with burrow mottles and faint color banding (Fig. 32).

Levee of Amazon Channel (Subunits IIIA and Upper Part of IIIB)

The levee of the Amazon Channel (i.e., the channel cored at Site 945) forms the upper 18 m of Site 946. Subunit IIIA (1.18–4.42 mbsf) comprises mud with numerous graded beds of fine sand to silt, on average 6 cm thick, making up 30% of the subunit. The upper part of Subunit IIIB (4.42–18 mbsf) contains bioturbated mud with numerous laminae and thin beds of silt.

Levee of an Older Channel of the Amazon System (Lower Part of Subunit IIIB and Upper Part of Subunit IIIC)

The lower 27 m of the morphological levee at Site 946 was deposited by overspill from a nearby earlier distributary of the Amazon system, which is located 2 km to the west of the Amazon Channel and Site 945. This older levee sequence corresponds to the base of Subunit IIIB and the top of Subunit IIIC. The base of Subunit IIIB (18–24.72 mbsf) consists of bioturbated mud with few silt laminae. The upper part of Subunit IIIC (24.72–45 mbsf) consists of mud with numerous silt laminae and a few graded beds of silt and sand. Sand beds 10–50 cm thick are rare.

Last-glacial Lower Fan (Lower Part of Subunit IIIC)

The lower part of Subunit IIIC (45–128.72 mbsf) corresponds to silt and sand beds on the lower fan over which the levees have pro-

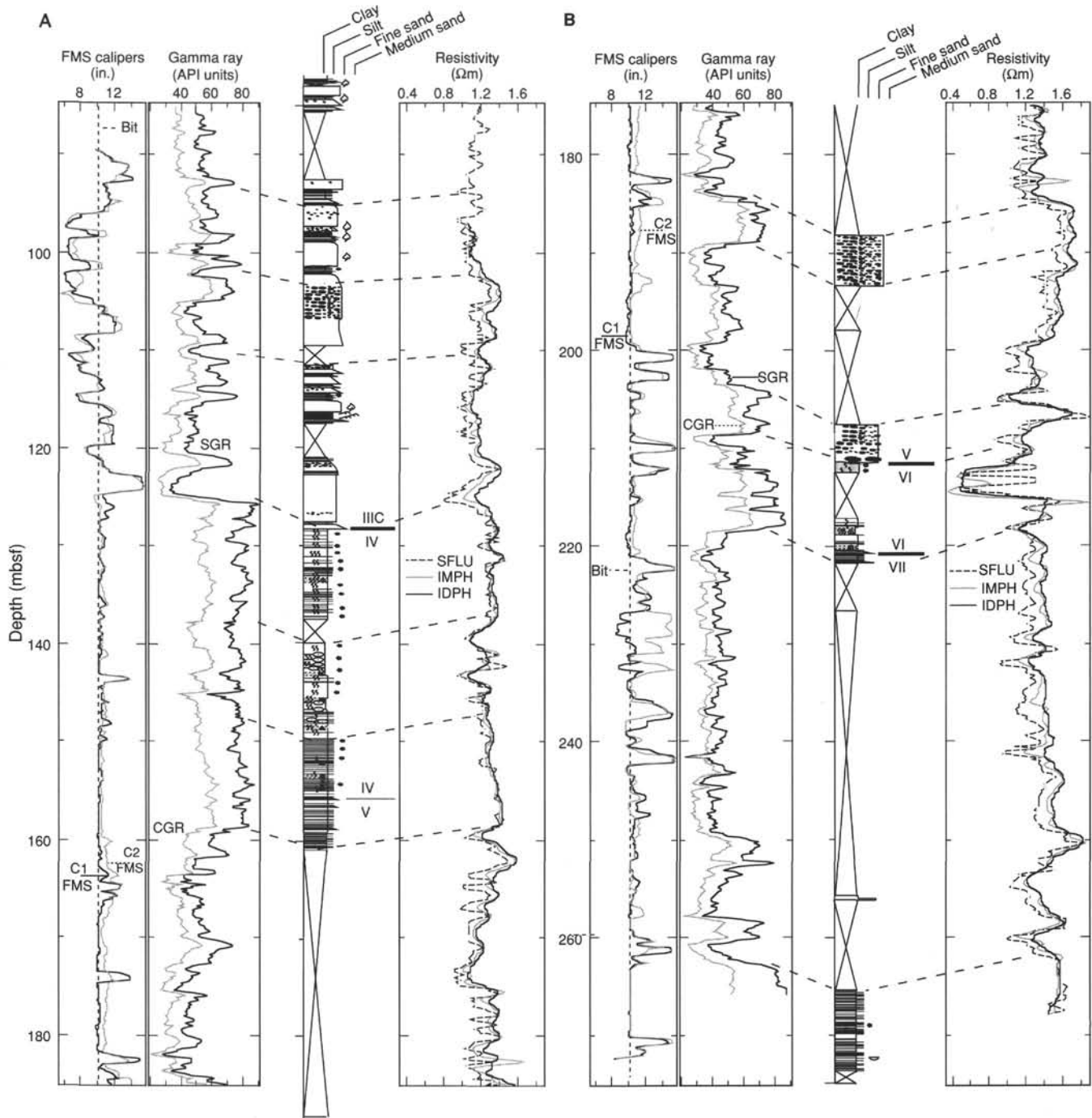


Figure 27. Comparison of caliper (from FMS), gamma-ray, and resistivity logs to lithologic description of cores for Hole 946A. An apparent offset exists between log and core depths of approximately 3 m over most of the interval logged. **A.** Upper section from 80 to 190 mbsf. **B.** Lower section from 170 to 275 mbsf.

graded. When deposited, this sand was located beyond the contemporary channel termination. The sediment consists of silt and sand beds, with some interbedded intervals of mud with silt laminae and thin beds. There is a general trend downhole to thicker sand beds and a higher proportion of sand with abundant mud clasts. Silt beds are as thick as 75 cm and are graded. Many sand beds have abundant 1- to 10-cm mud clasts, and all sand beds generally grade upward from poorly sorted fine sand to silt, although medium sand is present in a few beds. In some beds, the mud clasts are normally graded, whereas

in other beds they appear to be randomly distributed. Some mud clasts have clearly been folded or deformed. Some of the sand beds appear to be more than 1 m thick. The thickness of some sand beds may have been inflated by sand flow during coring. Intervals of high velocity and density values recorded on the wireline logs at 85–93, 115–125, and 121–129 mbsf correlate well with sand-rich beds recovered in the Hole 946A cores. (Note that all log boundaries appear to be 3 m higher than core depths). Intervals of sand with mud clasts show higher resistivity and gamma-ray response (e.g., 90–127 mbsf).

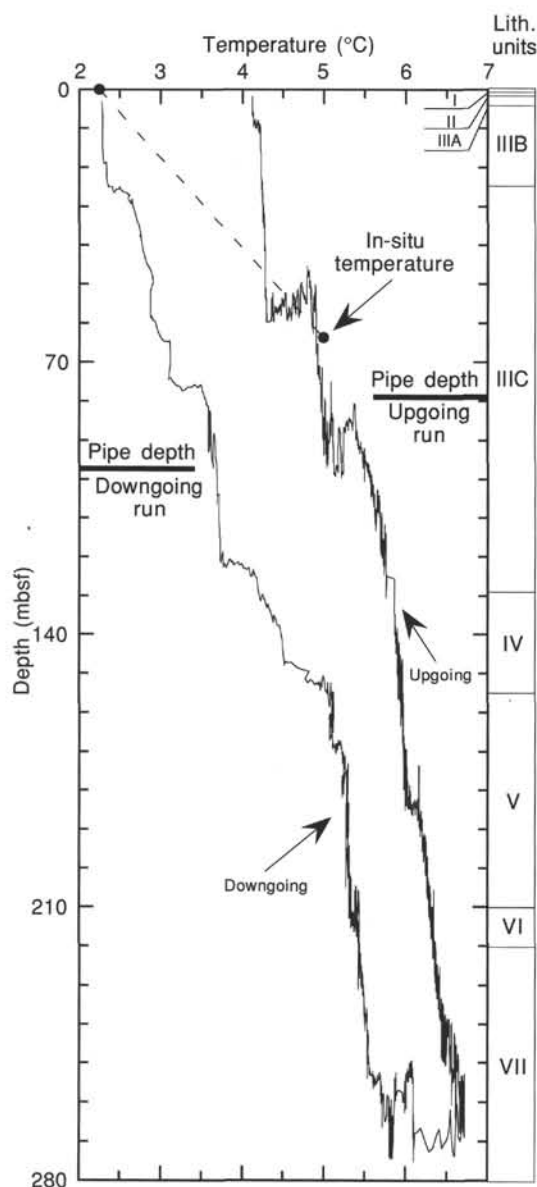


Figure 28. Borehole temperature log together with ADARA temperature measurements in Hole 946A. Lithostratigraphic units are given on right.

Last-interglacial Bioturbated Calcareous Mud (Unit IV)

Unit IV (128.72–155.82 mbsf) consists of a series of intervals of mud with silt laminae and minor beds of silt interspersed with beds of calcareous clay that have carbonate contents of 7%–36%. Burrow mottles are common to abundant throughout this unit. A thin calcareous clay occurs at 133.25–133.75 mbsf. From 140 to 149 mbsf, several 20- to 30-cm-thick intervals of greenish gray nannofossil-foraminifer clay alternate with dark gray foraminifer-bearing clay.

Lower Fan Sand and Distal Levees (Unit V)

Seismically, Unit V and the overlying Unit IV are correlated with the feather-edge of the Middle and/or the Lower Levee Complex. Unit V (155.82–211.37 mbsf) had only 21% recovery, and most of its sand was highly disturbed by coring. The upper 5 m of the unit comprises mud with thin to thick silt beds. Below this, recovery was

sparse and consists of two cores of abundant mud clasts set in a poorly sorted matrix of fine to medium sand. Wireline log data suggest that much of this unit consists of porous sand, which below 180 mbsf forms three coarsening-upward sequences. FMS images show packets of 0.5- to 1-m-thick sand beds. The data suggest that individual sand packets are thicker than in the lower part of Unit III, which was also logged, but muddy intervals are thicker and less silty in Unit V.

Older Interglacial Bioturbated Calcareous Mud (Unit VI)

Unit VI (211.37–220.0 mbsf) consists of alternating greenish gray calcareous clay and dark gray mud with laminae and thin beds of silt. Burrow mottling is common. The top of the unit is an irregular erosional surface, and the overlying sand contains rip-up clasts from this unit.

Mid-Pleistocene Lower Fan Sand and Distal Levees (Unit VII)

Unit VII (220.0–273.67 mbsf) had less than 19% recovery, almost all of which was in two cores from the top and base of the unit that consist of mud with silt laminae, similar to levee sequences recovered elsewhere during Leg 155. Wireline logs, however, show that from 218 to 250 mbsf, the unit consists predominantly of sand. From 250 to 262 mbsf, log response suggests alternating sand and mud in a thinning-upward sequence, which is underlain by a predominantly muddy sequence below 262 mbsf corresponding to the mud with silt laminae recovered in Core 946A-29X. FMS images suggest sand bed thicknesses of 3–5 m at the top of the unit, decreasing downhole.

Implications

Two anomalous intervals of remanence direction and intensity, interpreted as geomagnetic excursions, occur at 101.5 mbsf and 133.5 mbsf, the latter in an interval of calcareous clay. On the basis of the pattern of their remanence behavior, these are interpreted as the Lake Mungo (30 ka) Excursion and the Blake (105 ka) Event. Oscillations in paleomagnetic declination and inclination, interpreted as secular variation, are best developed from 10 to 13 mbsf, with a wavelength of 0.25 m.

Foraminifers and nannofossils are well preserved and abundant in the calcareous clays of Units I, IV, and VI. Otherwise, microfossils are sparse and nannofossils are commonly etched. The base of the Holocene was identified near the base of Unit II, inconsistent with its position at the top of Unit II at Site 943 further up Amazon Channel. *P. obliquiloculata* is found in a sandy interval at 53.5 mbsf in Unit III and is probably reworked; underlying cores do not contain this foraminifer and are many meters above the probable Lake Mungo paleomagnetic excursion.

Units IV and VI contain interglacial foraminifers including *G. menardii*, *G. tumida*, and *G. tumida flexuosa*. *G. hexagonus* is present in Unit IV. Unit IV nannofossil assemblages are of Zone CN15a similar to those in Units III, IV, and V at Site 942. Unit VI nannofossil assemblages are of Zone CN14b. They are dominated by *Gephyrocapsa*.

In the middle part of Unit V, the only sample recovered was a 10-cm-long core-catcher at 168 mbsf, which contained common foraminifers, including *G. tumida* and *P. obliquiloculata*. In the absence of any other recovery in this interval, it is unknown whether this represents in-situ interglacial sediment or a clast in a sand bed.

Site 946 is the only site to have recovered two major units containing interglacial calcareous clay beds, with a thick sandy interval (Unit V) between them. The presence of the geomagnetic Blake Event (105 ka) and the tentative biostratigraphic correlation with Site 942 allows us to correlate Unit IV with the interglacial of isotopic Stage 5. A similar assemblage is found in Unit III at Site 942 and in clasts in Unit III sand at Site 935 and in the Unit III debris-flow deposit at Site 944.

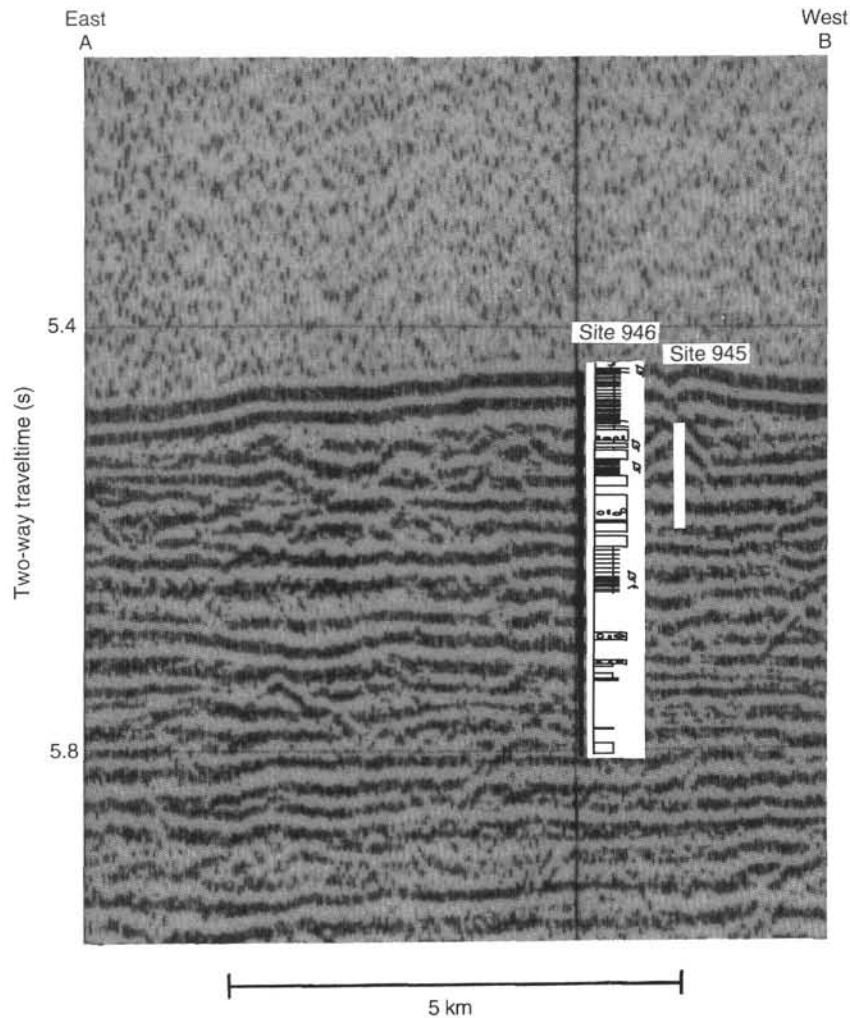


Figure 29. *JOIDES Resolution* water-gun seismic profile showing lithostratigraphic observations at Site 946. Location of profile in Figure 1 of “Site 945” chapter, this volume.

Units IV and VI have different nannofossil and foraminifer assemblages and are separated by a thick sand unit. Unit VI therefore dates from an earlier interglacial and correlates biostratigraphically with the interglacial sediment beds near the base of Sites 931 and 933. The CN14b nannofossil assemblage in the deep carbonate units overlying the Lower Levee Complex in Sites 935, 936, and 944 is apparently different both from (1) the CN14b assemblages at Sites 931, 933, and Unit VI of Site 946, and (2) the CN15a assemblages at Sites 942 and 946. Thus, we can tentatively identify three interglacial intervals in the sites that we have cored. The uppermost, corresponding to isotopic Stage 5, overlies the Middle Levee Complex. The second (? isotopic Stage 9) rests on the Lower Levee Complex. The third (? isotopic Stage 11) overlies the Bottom Levee Complex at Sites 931 and 933 and was sampled in Unit VI of Site 946.

The apparent lateral continuity of sandy units between Site 945 and the upper 110 m of Site 946 implies that these sand types have a sheet-like geometry thought to be typical of sand lobes beyond channel terminations. Similar sandy intervals characterize Units V and VII, with seismic-reflection profiles suggesting lateral continuity of sand packets. Based on logging data, sand in Unit V seems to form thickening-upward sequences. In places, these sandy units are intercalated with muds that contain laminae and beds of silt, representing distal levee deposition; these finer grained facies were preferentially recovered in cores. Some thick sand beds that contain abundant mud clasts may have originated at the time of avulsion up-fan by active

down-cutting through the old levee. Such beds have been found at the base of individual channel-levee systems at Sites 943 and 945.

Deposition at Site 946 may be broadly cyclical. Channel avulsion leads to deposition of a thick sand with abundant mud clasts. Subsequent sand deposition may form a thickening-upward sequence as a result of progradation of the active channel-levee system. Eventually, distal levee deposits prograde over the lower fan sand. The carbonate-rich muds presumably correspond to times of elevated sea level when Amazon River sediment was effectively trapped in near-shore and inner-shelf environments. All carbonate-rich muds have interglacial foraminiferal faunas.

Diagenetic processes at Site 946 appear similar to those at other sites. Pore-water sulfate goes to zero by 12 mbsf. In the carbonate units, the content of organic carbon (0.4%) and nitrogen (0.1%) is low compared with abundances in levee muds. Rare siderite concretions are found in Unit III.

Honeycomb structure was observed in some beds, and several sand layers showed unusually vigorous degassing, suggesting the possible presence of gas hydrates. However, no associated pore-water anomalies were found. Chlorinity is a little lower (545–548 mM) in all samples below 120 mbsf.

Between 14 and 23 mbsf, water content and related index properties remain virtually constant. A similar feature was observed in near-surface muds at Sites 939, 940, and 944. The origin of this undercompaction is uncertain.

REFERENCES*

Damuth, J.E., 1977. Late Quaternary sedimentation in the western equatorial Atlantic. *Geol. Soc. Am. Bull.*, 88:695-710.

Flood, R.D., Manley, P.L., Kowsmann, R.O., Appi, C.J., and Pirmez, C., 1991. Seismic facies and late Quaternary growth of Amazon submarine fan. In Weimer, P., and Link, M.H. (Eds.), *Seismic Facies and Sedimentary Processes of Submarine Fans and Turbidite Systems*: New York (Springer), 415-433.

Pirmez, C., 1994. Growth of a submarine meandering channel-levee system on the Amazon Fan [Ph.D. thesis]. Columbia Univ., New York.

*Abbreviations for names of organizations and publications in ODP reference lists follow the style given in *Chemical Abstracts Service Source Index* (published by American Chemical Society).

Ms 155IR-122

NOTE: For all sites drilled, core-description forms ("barrel sheets") and core photographs can be found in Section 4, beginning on page 703. Forms containing smear-slide data can be found in Section 5, beginning on page 1199. GRAPE, index property, magnetic susceptibility, and natural gamma data are presented on CD-ROM (back pocket).

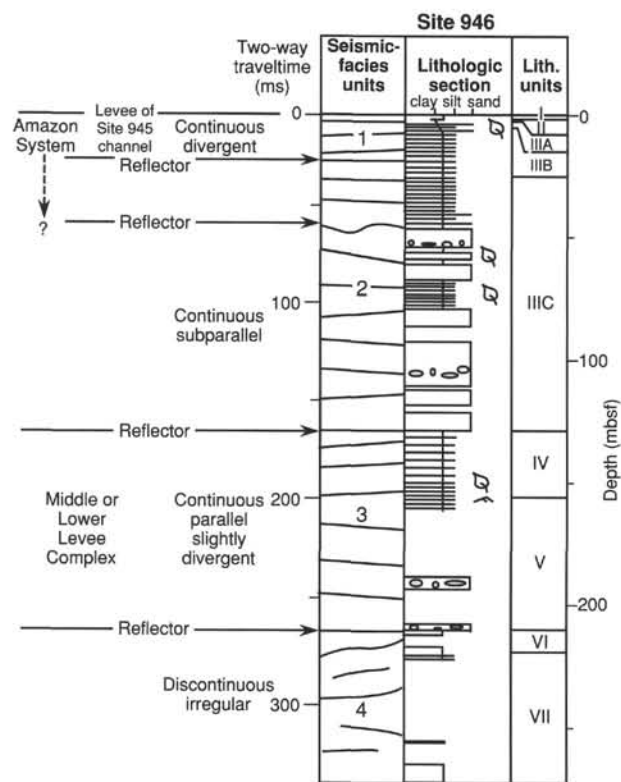


Figure 30. Correlation of lithostratigraphic observations with seismic-facies units and prominent reflections at Site 946.

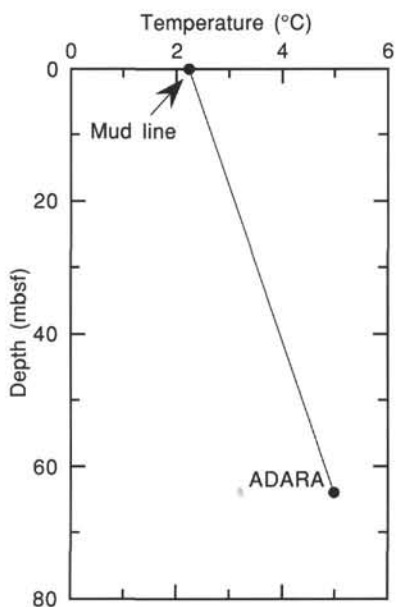


Figure 31. Estimated equilibrium temperatures in Hole 946A. A linear fit indicates a geothermal gradient of 42.92°C/km.

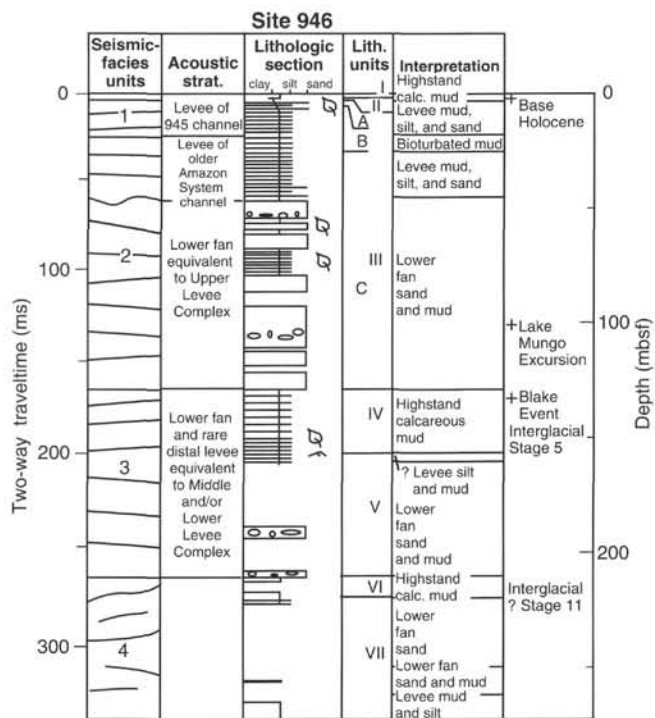


Figure 32. Summary of Site 946 showing (left to right) seismic-facies units, acoustic stratigraphy, schematic lithologic column, lithologic units, interpreted sediment facies, and chronological picks.

SHORE-BASED LOG PROCESSING

Hole 946A

Bottom felt: 4111.5 mbrf
Penetration: 275 mbsf
Total core recovered: 172.18 m (62.6%)

Logging Runs

Logging string 1: DIT/LSS/HLDT/CNTG/NGT

Logging string 2: FMS/GPIT/NGT (two passes)

Wireline heave compensator was used to counter ship heave.

Bottom-hole Assembly (BHA)

The following BHA depths are as they appear on the logs after differential depth shift (see **Depth shift** section below) and depth shift to the seafloor. As such, there might be a discrepancy with the original depths given by the drillers on board. Possible reasons for depth discrepancies are ship heave, use of wireline heave compensator, and drill string and/or wireline stretch.

DIT/HLDT/LSS/CNTG/NGT: BHA at 81.5 mbsf.

FMS/GPIT/NGT: BHA at 77.5 mbsf (main pass).

FMS/GPIT/NGT: recorded open hole (repeat pass).

Processing

Depth shift: All original logs have been interactively depth shifted with reference to NGT from FMS/GPIT/NGT (main run) and to the seafloor (-4111.5 mbrf). A list of the amount of differential depth shifts applied at this hole is available upon request.

Gamma-ray processing: NGT data have been processed to correct for borehole size and type of drilling fluid.

Acoustic data processing: No re-processing necessary due to the good quality of the logs.

Quality Control

During the processing, quality control of the data is mainly performed by cross-correlation of all logging data. Large (>12 in.) and/or irregular borehole adversely affects most recordings, particularly those that require eccentricization and a good contact with the borehole wall (CNTG, HLDT).

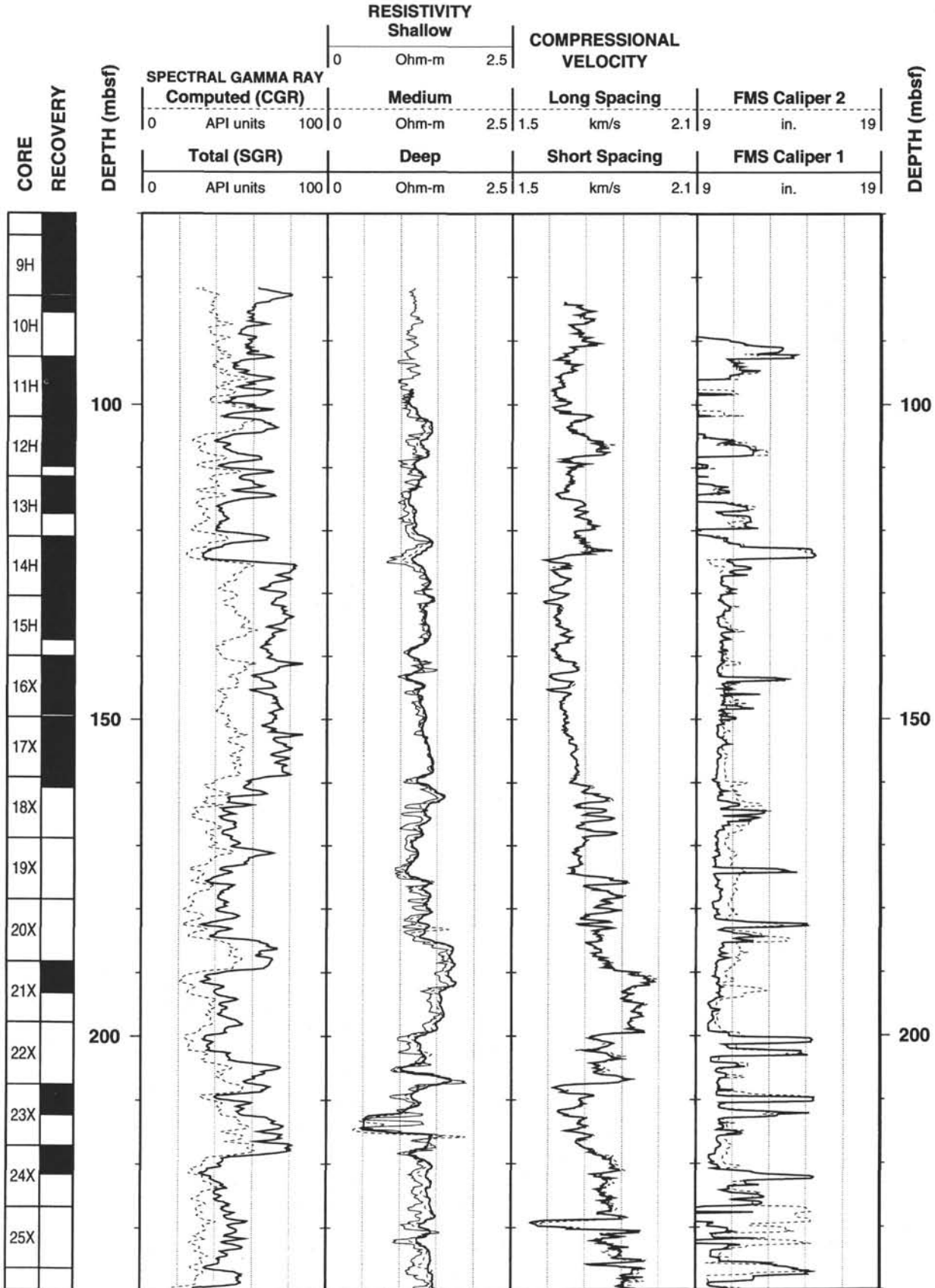
Hole diameter was recorded by the caliper on the FMS string (C1 and C2). The HLDT hydraulic caliper did not work properly during the main pass of the DIT/LSS/HLDT/CNTG/NGT and therefore the appropriate hole size correction could not be applied. The HLDT caliper, however, worked during the repeat pass, as shown by a comparison with the FMS caliper. Furthermore, a comparison of the density data from the repeat and the main passes shows almost identical curves, suggesting that despite the lack of a proper hole size correction the density recording in the main pass is of good quality. Data recorded through bottom-hole assembly, such as the NGT and CNTG, should be used only qualitatively because of the attenuation on the incoming signal.

NOTE: Details of standard shore-based processing procedures are found in the "Explanatory Notes" chapter, this volume. For further information about the logs, please contact:

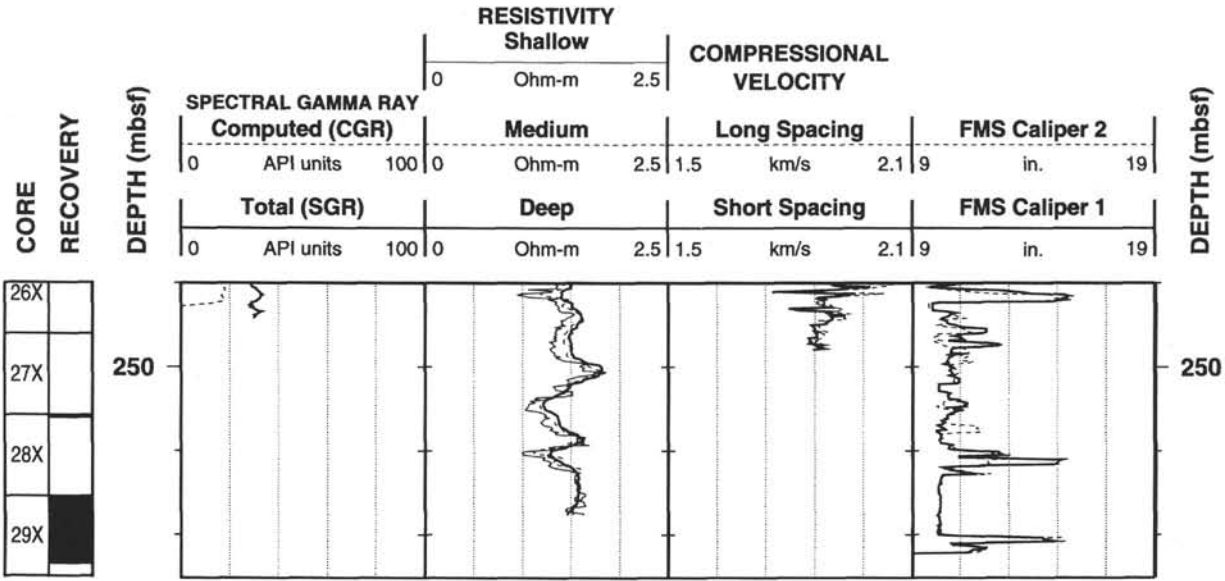
Cristina Broglia
 Phone: 914-365-8343
 Fax: 914-365-3182
 Email: chris@ldeo.columbia.edu

Elizabeth Pratson
 Phone: 914-365-8313
 Fax: 914-365-3182
 Email: beth@ldeo.columbia.edu

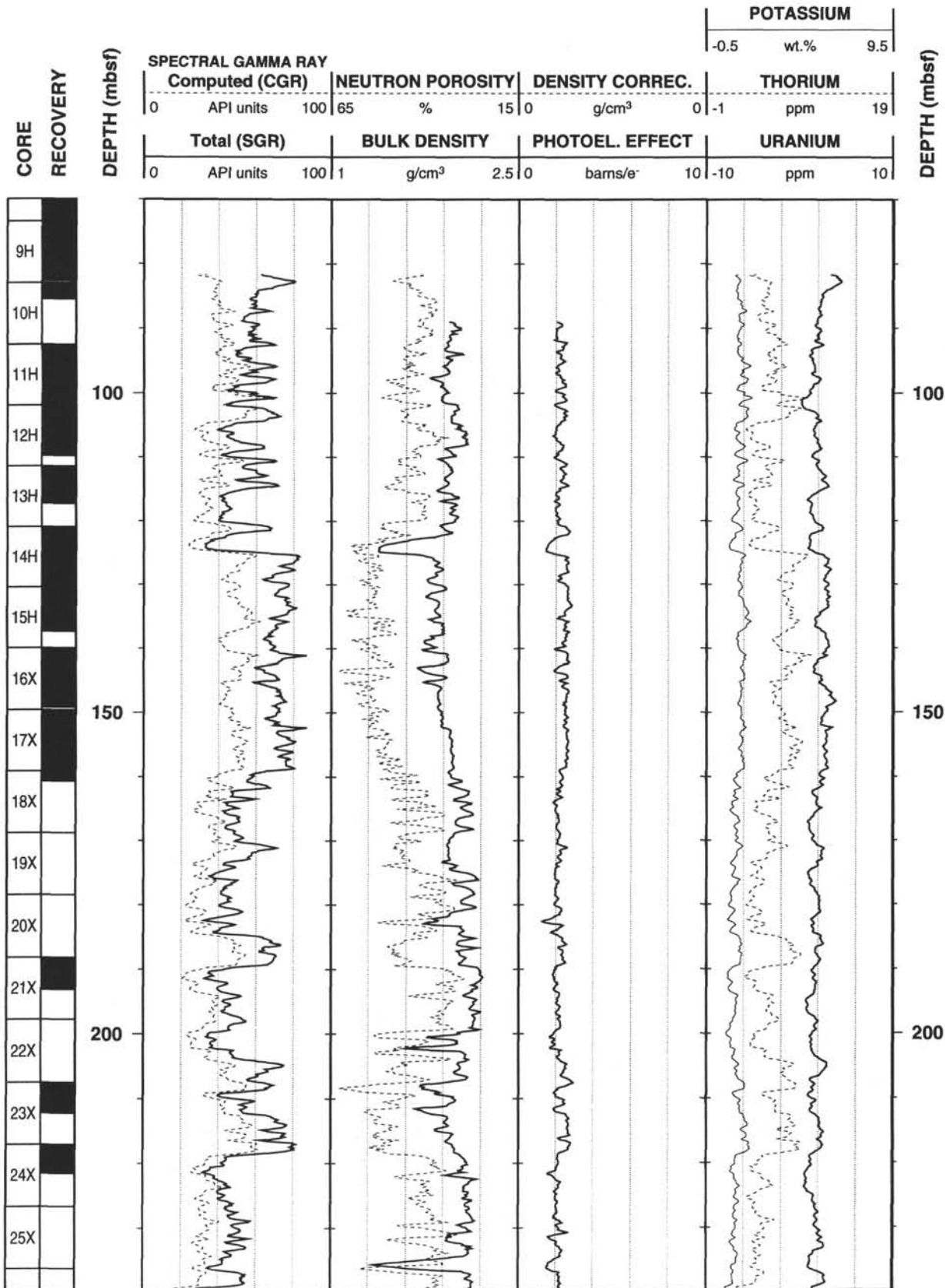
946A Natural Gamma Ray-Resistivity-Velocity Logging Data



946A Natural Gamma Ray-Resistivity-Velocity Logging Data (cont.)



946A Natural Gamma Ray-Density-Porosity Logging Data



946A Natural Gamma Ray-Density-Porosity Logging Data (cont.)

